

# 1 A new inventory of High Mountain Asia surging glaciers derived from 2 multiple elevation datasets since the 1970s

3 Lei Guo<sup>1</sup>, Jia Li<sup>1</sup>, Amaury Dehecq<sup>2</sup>, Zhiwei Li<sup>1</sup>, Xin Li<sup>3</sup>, Jianjun Zhu<sup>1</sup>

4 <sup>1</sup>School of Geo-science and Info-physics, Central South University, Changsha, 410083, China.

5 <sup>2</sup>Univ. Grenoble Alpes, IRD, CNRS, Grenoble INP, IGE, Grenoble, 38000, France.

6 <sup>3</sup>Institute of Tibetan Plateau Research, Chinese Academy of Sciences, Beijing, 100101, China.

7

8 *Correspondence to:* Jia Li (lijia20050710@csu.edu.cn)

9 **Abstract.** Glacier surging is an unusual instability of ice flow and complete surging glacier inventories are important for  
10 regional mass balance studies and assessing glacier-related hazards. Glacier surge events in High Mountain Asia (HMA) are  
11 widely reported. However, the completeness of present inventories of HMA surging glaciers is constrained by the insufficient  
12 spatial and temporal coverage of glacier change observations, or by the limitations of the identification methods. In this paper,  
13 we established a new inventory of HMA surging glaciers based on the glacier surface elevation changes and morphological  
14 changes over four decades. Four kinds of elevation sources (KH-9 DEM, NASADEM, COP30 DEM, HMA8m DEM), three  
15 elevation change datasets, and long-term Landsat image series were utilized to assess the presence of typical surge features  
16 over two time periods (1970s-2000 and 2000-2020). In total 890 surging and 336 surge-like glaciers were identified in HMA.  
17 Compared to the previous surging glacier inventories in HMA, our inventory incorporated 253 previously unidentified surging  
18 glaciers. The number and area of surging glaciers accounted for ~2.49% (excluding glaciers less than 0.4 km<sup>2</sup>) and ~16.59%  
19 of the total glacier number and glacier area in HMA, respectively. Glacier surges were found in 21 of the 22 subregions of  
20 HMA (except for the Dzhungarsky Alatau), however, the density of surging glaciers is highly uneven. Surging glaciers are  
21 common in the northwest subregions (e.g., Pamir and Karakoram), but scarce in the peripheral subregions (e.g., Eastern Tien  
22 Shan, Eastern Himalaya, and Hengduan Shan). The inventory further confirmed that surge activity is more likely to occur for  
23 glaciers with larger area, longer length, and wider elevation range. Among the glaciers with similar area, the surging ones  
24 usually have steeper slope than the non-surging ones. Besides, we found a potential relationship between the surging glacier  
25 concentration and regional glacier mass balance. The subregions with slightly negative or positive mass balance hold large  
26 clusters of surging glaciers, while those with severe glacier mass loss hold very few surging glaciers. The inventory and  
27 elevation change products of identified surging glaciers are available at: <https://doi.org/10.5281/zenodo.7590838> (Guo et al.,  
28 2022).

29 **Key words:** High Mountain Asia, Surging glacier inventory, elevation change, KH-9, Digital Elevation Model (DEM)

## 30 1 Introduction

31 A surge is a glacier instability that translates into an abnormally fast flow over a period of a few months to years (Cogley et  
32 al., 2011). A surging glacier exhibits an active phase (surge) and a quiescent phase that may occur at quasi-periodic intervals  
33 (Jiskoot, 2011). While a glacier enters into the surging states, a large volume of ice mass is transported downstream at a higher-  
34 than-average speed. In the quiescent phase, a glacier returns to a slow-moving state, and gradually regains mass in upper  
35 recaches. Previous studies pointed out that the surge-type glaciers only represent ~1% of total glaciers (Jiskoot, 2011; Sevestre  
36 and Benn, 2015). However, glacier surges are far more than an occasional behavior in some specific regions, such as the  
37 Alaska-Yukon (Clarke et al., 1986), Svalbard (Jiskoot et al., 2000; Farnsworth et al., 2016), and Karakoram-Pamir (Bhambri  
38 et al., 2017; Goerlich et al., 2020; Guillet et al., 2022). Glaciers in these regions have experienced heterogeneous mass loss in

39 the past decades (Hugonnet et al., 2021). How glacier surge activities impact the glacier regional mass balance needs further  
40 investigation, and to facilitate this kind of study, the glacier surges needed to be found out first.

41 In recent years, substantial efforts have been made to understand the mechanisms of glacier surges, including the hydrological-  
42 control(Kamb, 1987; Fowler, 1987), thermal-control(Fowler et al., 2001; Murray et al., 2003), environmental factor(Hewitt,  
43 2007; Van Wyk de Vries et al., 2022), friction state(Thøgersen et al., 2019; Beaud et al., 2021), and the unified enthalpy  
44 balance model (Sevestre and Benn, 2015; Benn et al., 2019). To support such studies, the accurate description of surging  
45 glacier distribution is needed to provide samples for studying the internal dynamic process of surges. Besides, glacier surge  
46 can induce several kinds of hazards, e.g., glacier lake outbursts (GLOF) (Round et al., 2017; Steiner et al., 2018), mudslides  
47 (Muhammad et al., 2021), or ice collapse (Kääb et al., 2018; Paul, 2019). Such mountain hazards have been frequently reported  
48 in recent decades (Shugar et al., 2021; An et al., 2021; Kääb et al., 2021). A complete inventory of surging glaciers is a basis  
49 for the regional hazard assessment of glacier surges.

50 Generally, a surging glacier could exhibit either one or several drastic changes, including: extreme speed-up (by a factor  
51 10~1000 compared to normal conditions), distinct elevation change pattern, rapid terminus advance, and surface  
52 morphological changes (medial or looped moraine, crevasses, etc.) (Jiskoot, 2011). The identification of surging glaciers can  
53 be implemented based on the observation of the above changes, e.g., glacier surface morphology (Clarke et al., 1986; Paul,  
54 2015; Farnsworth et al., 2016), terminus position (Copland et al., 2011; Vale et al., 2021), or glacier motion (Quincey et al.,  
55 2011). As for the surge-type glacier, which refers to the glacier that possibly surged prior to the observation period, are  
56 generally identified by the indirect morphological evidence (without observed changes) (Goerlich et al., 2020). The visual  
57 interpretation of glacier surface morphological changes is easy to operate, but fraught with uncertainty due to the snow cover  
58 or the absence of supraglacial moraine (Jacquemart and Cicoira, 2022). To recognize abnormal changes in glacier motion, a  
59 long-term flow velocity time series is needed (Yasuda and Furuya, 2015; Round et al., 2017). Since the quiescent phase may  
60 last for decades and the image source for estimating the flow velocity is limited, the abnormal changes in glacier motion are  
61 prone to be missed. By contrast, the recognition of abnormal surface elevation changes is an effective way to identify the  
62 surging glaciers, which has been confirmed by several glacier mass-balance studies (Bolch et al., 2017; Zhou et al., 2018), as  
63 its source datasets can satisfy the requirement of spatial-temporal coverage with comparatively fewer acquisitions. By  
64 combining observations of multiple features, the identification of surging glaciers could be more efficient and complete  
65 (Mukherjee et al., 2017; Goerlich et al., 2020; Guillet et al., 2022). However, when conducting such studies on a large spatial  
66 scale or a long temporal scale, one should select the least time-consuming but effective identification method. In that case, it's  
67 ideal to take the long-term elevation change as the criteria, and to combine with other observations as complements if possible  
68 (Guillet et al., 2022).

69 Except for the polar regions, High Mountain Asia (HMA) is the most densely glacierized region in the world. Within the HMA  
70 range, several subregions are famous for the concentration of surging glaciers as well as the anomalous glacier mass balance  
71 (Hewitt, 2005; Gardelle et al., 2013; Farinotti et al., 2020). The inventories of surging or surge-like glaciers have been  
72 established for some subregions like the Karakoram (Bhambri et al., 2017), West-Kunlun (Yasuda and Furuya, 2015), Pamir  
73 (Goerlich et al., 2020), Tien Shan (Mukherjee et al., 2017; Zhou et al., 2021). Sevestre and Benn (2015) presented the first  
74 global surging glacier inventory by reanalyzing historical reports from 1861 to 2013. However, it was compiled from various  
75 data sources (publications, reports, etc.) with inconsistent spatial-temporal coverage, which makes it difficult to ensure  
76 accuracy and completeness. Vale et al. (2021) identified 137 surging glaciers across HMA by detecting surge-induced terminus  
77 change and morphological changes from Landsat images from 1987 to 2019. The number is obviously underestimated, because  
78 it is smaller than the numbers of previous subregional inventories (Bhambri et al., 2017; Goerlich et al., 2020). Guillet et al.  
79 (2022) presented a new surging glacier inventory of HMA by identifying multiple glacier change features. In total 666 surging  
80 glaciers were identified across HMA. However, the glacier change observation period is shorter than two decades (2000-2018),  
81 and therefore some surging glaciers with relatively long revisit cycles may be missed.

82 In this study, we aimed to build a new inventory to include more surging glacier within HMA based on glacier surface elevation  
83 change observations over four decades. A workflow was developed to obtain the historical glacier surface elevation change  
84 from multiple datasets, including the KH-9 DEM (1970s), NASADEM (2000), COP30 DSM (2011-2014), HMA8m DEM  
85 (2002-late 2016), and previously published elevation change datasets. Glaciers in the new inventory were divided into three  
86 classes of confidence in surge detection. After that, the elevation change based inventory were further completed and corrected  
87 by the identification of morphological changes in a long-term timeseries of Landsat images (1986-2021). Based on the present  
88 inventory, the distribution and geometric characteristics of surging glaciers within HMA were statistically analyzed, in order  
89 to demonstrate their spatial heterogeneity and geometrical difference from the normal glaciers.

## 90 **2 Study region**

91 High Mountain Asia consists of the Qinghai-Tibet Plateau and the surrounding regions, including the Karakoram, Pamir,  
92 Himalayas, and Tien Shan. According to the updated Glacier Area Mapping for Discharge from the Asian Mountains  
93 (GAMDAM2) glacier inventory, HMA hosts 131819 glaciers, covering a total area of ~99817 km<sup>2</sup> (Sakai, 2019). The Hindu  
94 Kush Himalayan Monitoring and Assessment Programme (HiMAP) divided HMA into 22 subregions (Fig. 4) (Bolch et al.,  
95 2019). Different subregions are influenced by different climate regimes, such as the South Asia monsoon, the East Asia  
96 monsoons, and the westerlies (Bolch et al., 2012; Maussion et al., 2014). Glacier mass balance across HMA was found to be  
97 heterogeneous in the past decades (Gardelle et al., 2013; Brun et al., 2017; Shean et al., 2020). In particular, glaciers in the  
98 Pamir-Karakoram-West Kunlun region had a slightly positive or balanced mass budget (Hewitt, 2005; Zhou et al., 2017;  
99 Farinotti et al., 2020), while those in the Eastern Himalayas, Nyainqentanglha and Hengduan Shan mountain ranges  
100 experienced substantial ice loss (Maurer et al., 2019).

## 101 **3 Datasets**

### 102 **3.1 Elevation Data**

103 The NASADEM is mainly reprocessed from the C-band SRTM (Shuttle Radar Topography Mission) images. Among the  
104 current global DEMs, the NASADEM has the shortest source data acquisition period (~11/02/2000~22/02/2000) (Farr et al.,  
105 2007). Based on an improved production flow, the NASADEM has a better performance than the earlier SRTM void-free  
106 product in most regions (Crippen et al., 2016). The NASADEM was employed as the reference elevation source because its  
107 acquisition time, 2000, is suitable to divide the elevation change observations to before and after 21st century with moderate  
108 time span (one or two decades). Each tile of the product has an extent of 1°× 1° and a pixel spacing of 1 arc-second (see Fig.  
109 1a). In total 313 tiles were downloaded from NASA LP DAAC  
110 ([https://e4ftl01.cr.usgs.gov/MEASURES/NASADEM\\_HGT.001/](https://e4ftl01.cr.usgs.gov/MEASURES/NASADEM_HGT.001/)).

111 Another global DEM we utilized is the newly released Copernicus DEM GLO-30-DGED (i.e., COP30 DEM). The COP30  
112 DEM was edited from the delicate WorldDEM™, which was generated based on the TanDEM-X mission. The global RMSE  
113 of COP30 DEM is ± 1.68 m (AIRBUS, 2020). Several studies have pointed out that this DEM is the most reliable open-access  
114 DEM to date (Purinton and Bookhagen, 2021; Guth and Geoffroy, 2021). The source images of COP30 DEM were mostly  
115 acquired between 2011 and 2014, and therefore COP30 DEM is suitable to represent the surface elevation in the 2010s. Like  
116 the NASADEM, the COP30 DEM has a pixel spacing of 1 arc second. Each tile of product has an extent of 1°× 1°. In total  
117 313 tiles were downloaded through ESA Panda (<https://panda.copernicus.eu/web/cds-catalogue/panda>).

118 The High Mountain Asia 8-meter DEM (HMA8m DEM) was also utilized in this study. The HMA8m DEM was generated  
119 from high-resolution commercial optical satellite stereo images, including WorldView-1/2/3, GeoEye-1, and Quickbird-2  
120 (Shean et al., 2020), through an automated photogrammetry workflow that is integrated with multiple error-control processes

121 (Shean et al., 2016). This DEM was originally produced for the mass balance estimation of HMA glaciers, so it covered most  
122 of the glacierized regions in HMA. In total 3598 DEM tiles were downloaded from National Snow and Ice Data Center  
123 ([https://nsidc.org/data/HMA\\_DEM8m\\_MOS/versions/1](https://nsidc.org/data/HMA_DEM8m_MOS/versions/1)). About 95% of them were acquired between 2010 and 2016 (Fig. 1b).  
124 Due to the data voids and inconsistent acquisition time, the HMA8m DEM was taken as a supplementary elevation source to  
125 increase the observations in the 2010s.

126 The Hexagon KeyHole-9 (KH-9) imagery was acquired in the 1970s. It is one of the earliest near-global satellite stereo image  
127 source. The KH-9 imagery is characterized by a spatial resolution of 6-9 m, a wide coverage (130 km x 260 km), and a 70%  
128 forward overlap (Surazakov and Aizen, 2010). Many studies have utilized this imagery to estimate historical glacier surface  
129 elevation (Holzer et al., 2015; Zhou et al., 2017; Maurer et al., 2019). The KH-9 DEMs used in this study were generated  
130 through the automated ASPy pipeline (Dehecq et al., 2020). The methodology, validated in the European Alps and Alaska  
131 achieved a vertical accuracy of ~5m (68% confidence level). For more details on the method of KH-9 DEM generation, please  
132 refer to Dehecq et al. (2020). In total 238 DEMs with a resolution of 48 m were generated from the KH-9 images acquired  
133 between 1973 and 1980. The KH-9 DEMs were utilized to represent the glacier surface elevation in the 1970s (See Fig. 1c).  
134 Several newly published elevation change datasets were also collected to include the most recent surges as much as possible  
135 (Brun et al., 2017; Shean et al., 2020; Hugonnet et al., 2021). We mainly used the elevation change results presented by  
136 Hugonnet et al. (2021) to extend the observation period to 2020, which has a resolution of 100 m and a temporal interval of 5  
137 years. Through the inter-comparison of the multiple elevation change results, the gross errors or false signals in the elevation  
138 change patterns could be easily detected.

### 139 **3.2 Optical Satellite Images**

140 In order to assist the identification of surging glacier, we also identified morphological changes associated with surges in multi-  
141 temporal optical satellite images. We mainly relied on the 1986-2021 Landsat imagery to capture the glacier morphological  
142 changes. We downloaded the false-colour composited Landsatlook images with 30m resolution (geo-referenced) that have  
143 good brightness contrast over snow/ice areas from USGS website (<https://earthexplorer.usgs.gov>). The images were pre-  
144 selected to satisfy the requirement of cloud cover (<10%). In total, 7843 Landsatlook images in 148 frames were used (see Fig.  
145 1d). We also utilized the very high-resolution (VHR) images (Google/ESRI/Bing, etc.) as complements for surging feature  
146 identification. The fine resolution of these images allows us to visually check the possible morphological features caused by  
147 past surges.

### 148 **3.3 Glacier inventory**

149 In this study, we used the GAMDAM2 glacier inventory (Sakai, 2019) as template for the surging glacier inventory, rather  
150 than the Randolph Glacier Inventory V6.0 (RGI6.0) (RGI Consortium, 2017). The GAMDAM glacier inventory has included  
151 many small glaciers that are missed in RGI6.0, and provides a more accurate glacier extent by excluding outcrop rocks and  
152 shaded areas (Nuimura et al., 2015). Since the GAMDAM2 inventory only contains the glacier polygon vectors, we calculated  
153 the geometric and topographic attributes for each glacier in a way similar to that of RGI6.0. The maximum glacier centreline  
154 was calculated through the Open Global Glacier Model (OGGM) (Maussion et al., 2019). The attributes were used to interpret  
155 the geometric characteristics of surging glaciers.

## 156 **4 Methodology**

### 157 **4.1 Estimation of glacier surface elevation change**

158 The four kinds of DEMs have different coordinate references, vertical references, and data formats. Firstly, all DEMs were  
159 converted to float GeoTiff format. For datasets with quality files (NASADEM and the COP30 DEM), the DEM were

160 preprocessed to mask out the pixels of low quality. The poor pixels of COP30 DEM tile were determined through the attached  
161 height error map (with values larger than 2.5 m) and water body map (with values not equal to zero). The NASADEM was  
162 directly masked with the attached water mask file. Subsequently, the coordinate system, map projection, and vertical reference  
163 of all DEMs tiles were unified as the WGS84 coordinate system, HMA Albers Equal Area projection (Shean et al., 2020), and  
164 WGS84 ellipsoid. The glacier surface elevation changes during 2000-2010s were derived by subtracting the NASADEM from  
165 the COP30 DEM and HMA8m DEM, and those during 1970s-2000 were derived by subtracting the KH-9 DEM from the  
166 NASADEM.

167 An automated DEM differencing workflow for large-scale glacier surface elevation change estimation was developed based  
168 on the *demcoreg* package presented by Shean et al. (2019). The workflow integrated multiple DEM co-registration approaches,  
169 the polynomial fit of tilt error, and other adaptive outlier removal approaches that was operated based on the observations over  
170 stable regions. Hence, a mask that excluded the water bodies and glacierized regions was generated in advance. Before  
171 differencing, the two DEMs need to be co-registered, because a small geolocation shift can result in considerable elevation  
172 change errors in high mountain regions. The efficient analytical DEM co-registration method presented by Nuth and Kääb  
173 (2011) was used to eliminate the relative geolocation shift between DEMs. This method assumes the geolocation shift vectors  
174 of all DEM pixels are identical. However, for the global DEM products like NASADEM and COP30 DEM, a DEM tile was  
175 usually mosaiced from multiple DEM patches, and the geolocation shift vectors at different parts of the DEM tile may be  
176 different. In view of this problem, we developed a block-wise version of the analytical DEM co-registration method to reduce  
177 the impacts of geolocation accuracy anisotropy of a DEM tile. Each DEM tile was divided into  $m \times n$  blocks, and the DEM  
178 shifts were estimated for each block. Then, the  $m \times n$  groups of shift parameters were merged into one group of shift parameters  
179 through a cubic interpolation. Technically, the estimated shift parameters become increasingly representative as the block size  
180 decreases. However, the fitting of shift parameters requires a certain number of samples. The final block size was set to  
181  $300 \times 300$  pixels to reach the best balance between the representativeness and estimation accuracy of shift parameters. Besides,  
182 we found that the block-wise co-registration method could result in wrong fitting of shift parameters over flat regions. To deal  
183 with this, a threshold of mean slope ( $10^\circ$ ) was set to classify the DEMs into the flat and the hilly categories, and the original  
184 global co-registration method (Nuth and Kääb, 2011) was applied to the flat ones.

185 Due to the residual orbital error of satellite images, the elevation difference maps often showed planimetric trends. This type  
186 of systematic error was fitted as a universal surface trend using a quadratic polynomial model based on the observations in  
187 stable regions, and then was removed from the elevation difference tile (Li et al., 2017). Besides, due to the jitter of the SAR  
188 antenna and optical mapping camera, the elevation difference maps often showed stripes (i.e., band-like artifacts) (Yamazaki  
189 et al., 2017). To eliminate the stripes, the elevation difference map was converted to the frequency domain through the Fast-  
190 Fourier-Transform method. Since the cyclic values have a high frequency in the power spectral density map, a threshold of  
191 frequency was set to separate the stripes components from the normal elevation differences. The de-stripping was completed  
192 after the backward transformation. Finally, the outliers of elevation difference maps were reduced through the 3-sigma  
193 threshold criteria.

194 The radar penetration into glacier surface can result in biases of elevation change estimation, which could be several to dozens  
195 of meters, and potentially can lead to the false positive identification. We adopted a two-step procedure to reduce the radar  
196 penetration bias in the final elevation change results. First, we used the DEM differencing workflow mentioned above to  
197 subtract the NASADEM from the SRTM-X DEM. The elevation differences over glacierized area were regarded as the  
198 penetration difference between X-bands and C-bands. Secondly, we fitted a 3rd polynomial function between the glacial dH  
199 and altitude, which was deemed as the penetration depth – altitude relationship. Then, the radar penetration biases were  
200 removed from the COP30 DEM related results by taking the glacier elevation as input for the function. For the dH results  
201 calculated by differencing NASADEM and optical DEMs (e.g. HMA8m and KH-9 DEM), the penetration difference of X-

202 and C- bands was multiplied by 2 to represent the absolute penetration depth of C-band (Abdel Jaber et al., 2019; Fan et al.,  
203 2022) and then removed from the related results.

204 Finally, three elevation change maps were calculated: the COP30 DEM – NASADEM, the HMA8m DEM – NASADEM, and  
205 the NASADEM – KH-9 DEM. The first two elevation change maps were combined with the three elevation change datasets  
206 for surging glacier identification during the period 2000-2020, and the last one during the period 1970s-2000. In total, our  
207 elevation change observations covered ~92% of the total glacier area within HMA in 2000-2020, and ~77% in 1970s-2000.  
208 Gaps in observations were mainly due to: 1) data voids and incomplete coverage of original DEMs tile, which was the main  
209 cause for the KH-9 DEMs and HMA8m DEM related results; 2) gross error removal during the elevation change calculations,  
210 which led to the scattered holes in the COP30 DEM related results.

### 211 4.3 Surging glacier identification

212 The identification of surging glaciers in this study were divided into three steps. First, we generated a raw inventory of surging  
213 glaciers through the qualitative interpretation of multi-temporal elevation changes. Then, the visual identification of  
214 morphological changes was carried out for the identified surging and surge-like glaciers. This procedure can further confirm  
215 the surges or correct the false identifications based on glacier elevation changes (Guillet et al., 2022). The identified results  
216 were re-checked by careful inspection on VHR images, and by comparing with existed surging glacier inventory. Also, the  
217 surging tributaries were separated from the non-surging glacier trunk at this step.

#### 218 4.3.1 Identification through elevation changes

219 In general, a typical glacier surge cycle can be divided into three phases (Jiskoot, 2011): 1) the build-up phase, characterized  
220 by remarkable thickening in the upper reaches; 2) the active phase, characterized by remarkable thinning in the upper reaches  
221 and thickening in the lower reaches; 3) the post-surge phase, characterized by strong down-wasting in the lower reaches. The  
222 classical method of identifying surging glaciers is to recognize the combination of marked upper thinning and lower thickening  
223 in the longitudinal direction. However, to distinguish the surging glaciers in the build-up or post-surge phase, careful  
224 comparison with surrounding glaciers is required, which is difficult to be carried out with a mathematical index. In this study,  
225 we established a three-class indicator to distinguish the surge possibility through the visual interpretation of glacier elevation  
226 change patterns:

227 I) “verified”:

- 228 - a) obvious thickening in lower reaches (e.g. +30 m);
- 229 - b) contrasting upper-thinning (e.g. +20 m) and lower-thickening (e.g. +20 m);
- 230 - c) contrasting upper-thickening (e.g. +20 m) and lower-thinning (e.g. -30 m);
- 231 - d) severe thinning in the lower reaches (two time stronger than that of the normal glaciers, or comparable to the  
232 ablation of adjacent “verified” surging glaciers);

233 II) “probable”:

- 234 - a) moderate upper thinning (e.g. -15m) and lower thickening (e.g. +15m);
- 235 - b) only moderate thickening in the middle reaches (e.g. +15m);

236 III) “possible”:

- 237 - a) only moderate thickening at the terminus (e.g. +15m);
- 238 - b) only strong thinning in the lower reaches (one time stronger than adjacent normal glaciers).

239 Note that, the specific values of elevation change mentioned above were for information only. Because of the diversity in the  
240 regional elevation change patterns under different climate or topographic conditions, the thresholds may vary spatially.

241 The identification of surging glaciers was conducted separately in the two observation periods (1970s-2000 and 2000-2020).

242 The sub-inventory covering the period 1970s-2000 was generated based on the dH results of NASADEM – KH-9 DEM. For

243 the sub-inventory covering the period 2000-2020, its dH datasets contain the COP30 DEM – NASADEM, the HMA8m DEM  
244 – NASADEM, and three previously published elevation change datasets (Brun et al., 2017; Shean et al., 2020; Hugonnet et  
245 al., 2021). Within each observation period, each glacier will be labelled with its possibility level of surging and elevation  
246 change pattern in the attribute table. For example, the label of “I-c” means this glacier was classified as “verified” surging  
247 glaciers because contrasting upper-thickening and lower-thinning pattern were observed in the corresponding period. Figure 2  
248 shows an example of surging glacier identification result.

#### 249 **4.3.2 Identification through morphological changes**

250 Long-term Landsat images (acquired between 1986 and 2021) were utilized to investigate the morphological changes of the  
251 three types of potential surging glaciers identified from elevation change. With each Landsat image acquisition frame, all  
252 Landsatlook images of different dates (acquired from 1986 to 2021) were merged into an animated time-series image. Based  
253 on the animated image, we are able to easily identify the morphological changes. Due to the moderate resolution of Landsat  
254 images, only three types of feature changes were utilized as criteria for identifying glacier surges: terminus position change,  
255 looped moraine changes, and medial moraine changes. Similarly, we assigned a two-level index to each morphological change  
256 to indicate our confidence at the identification, which was defined as follow:

257 1) terminus advance:

258 I) : obvious terminus advancing (e.g. over 500 m);

259 II): small terminus advancing ( e.g. 0~500 m);

260 2) looped/medial moraine change:

261 I) : fast formation/vanishment of the looped moraine, or obvious distortion of the medial moraine;

262 II) : slow formation or vanishment of the looped moraine, or slight shape changes of existed looped moraine, or  
263 slight distortion of the medial moraine.

264 Each of the three kinds of morphological changes were individually qualified and labelled in the attribute table.

#### 265 **4.3.3 Generation of surging glacier inventory**

266 Through the above identification steps, in total five indicators were compiled to describe the changes of possible surging  
267 glaciers. The two sub-inventories of dH identified results were merge firstly following the principle of possibility, i.e., if a  
268 glacier was identified as a surging glacier in both periods but associated with different indicators, its indicator in the final  
269 inventory was taken from the indicator having a higher possibility. The possibility of indicators follows the order: “verified” >  
270 “probable” > “possible”. For example, a glacier was identified as a “verified” surging glacier in the period 1970s-2000, and  
271 was identified as a “probable” surging glacier in the period 2000-2010s, then it was qualified as a “verified” surging glacier.  
272 After that, the merged dH indicators were further compared with the morphological indicators to determine the final indicator  
273 of surge possibility. The “probable” or “possible” class was changed to a class with higher possibility (e.g., from “probable”  
274 to “verified”) only if a “I” kind of morphological change was found.

275 We think the advancing glaciers usually have such features: 1) only thickened in a small area at terminus, without contrasting  
276 upper thinning; 2) the advancing distance is relatively short (Lv et al., 2019, 2020; Goerlich et al., 2020). These features are  
277 corresponding to the “III-a” type of elevation change, and “II” type of terminus advance. Therefore, if a glacier only shows  
278 these two kinds of changes, it will be qualified as an advancing glacier, rather than a surging glacier.

279 For glacier complexes in which a tributary surged but the main trunk did not show any features of surge, such as the Biafo  
280 glacier, Fedchenko Glacier and Panmah Glacier (Hewitt, 2007; Goerlich et al., 2020; Bhambri et al., 2022), it’s necessary to  
281 separate the surging tributary from the trunk. A tributary will be considered as an individual surging glacier if it has the  
282 following features. Firstly, the transition of contrasting elevation change is located in this tributary. Secondly, the mass

283 contributed by this tributary to the glacier trunk is relatively small. Then we manually edited the outline to separate the tributary  
284 from the glacier complex. This kind of surges was also marked by the attribute of “trib\_surge”.  
285 In the final step, we inspected the identified surging glaciers on VHR imagery. The inspection aimed to remove the wrong  
286 identification due to some false signals, such as the severe lower-thinning in a lake-terminating glacier and remarkable surface  
287 heightening caused by nearby landslide. We also refined our inventory after careful comparison with inventories presented by  
288 Guillet et al. (2022), Goerlich et al. (2020) and Bhambri et al. (2017).

## 289 **5 Results**

### 290 **5.1 Identified surging glaciers**

291 A total of 1226 surge-related glaciers across the HMA were identified based on the elevation changes and morphological  
292 changes. The identified surge-related glaciers consisted of 890 ‘verified’ surging ones, 208 ‘probable’ ones, and 128 ‘possible’  
293 ones. A total of 175 surging tributaries were identified in 86 glacier complexes. When merging the identification results of the  
294 two periods, we found that a considerable proportion of identified surging glaciers were simultaneously recognized in two  
295 periods. This makes our inventory more reliable, since a surging glacier could exhibit different kinds of changes in different  
296 periods. For example, 26 probable and 51 possible surging glaciers identified during 2000-2020 turned to be “verified” surging  
297 glaciers during 1970s-2000. Meanwhile, 60 “probable” and 21 “possible” surging glaciers identified during 1970s-2000 turned  
298 out to be ‘verified’ surging glaciers during 2000-2020. Thanks to an almost complete coverage of the elevation change  
299 observations, we were able to classify all glaciers in HMA. Table 1 shows the number of surging glaciers identified from two  
300 periods of elevation changes and morphological changes. Due to the incomplete coverage and data voids of KH-9 DEMs,  
301 fewer surging glaciers were identified during the period 1970s-2000. The “probable” and “possible” classes were deemed as  
302 surge-like glaciers. To avoid confusion, only the “verified” surging glaciers were used for analysis and comparison throughout  
303 the rest of this study.

### 304 **5.2 Distribution of surging glaciers**

305 Surging glaciers were identified in 21 subregions of HMA (except for the Dzhungarsky Alatau), however, the density of  
306 identified surging glaciers is far from even (Fig. 3). Glacier surges are common in the northwest regions, sporadic in the inner  
307 regions, and scarce in the peripheral regions. Figure 4 and Table 2 show the ratios of surging glacier number and area in each  
308 subregion. Considering the area of the smallest identified surging glacier is 0.42 km<sup>2</sup>, we only took the glaciers larger than  
309 0.40 km<sup>2</sup> in the glacier number related ratio. When conducting statistical analysis, the surge-like glaciers were excluded from  
310 the dataset, and a surging tributary was regarded as an individual glacier. The number (890) and area (16556.42 km<sup>2</sup>) of  
311 identified surging glaciers accounted for ~2.49% and ~16.59% of the total glacier number and glacier area in HMA,  
312 respectively.

313 Among the 22 subregions, the Karakoram is the largest cluster of surging glaciers. In total 354 surging and 128 surge-like  
314 glaciers were identified in the Karakoram. The number and area of verified surging glaciers in the Karakoram accounted for  
315 39.80% and 47.90% of the total identified surging glaciers within HMA. We found more than half of the tributary surges (101)  
316 occurred in the Karakoram, where large glaciers are much more developed than other regions. In the Karakoram, although  
317 surging glaciers have only accounted for 8.59% of the total glacier number, their area occupied 39.48% of the total glacierized  
318 area. The Pamirs, composed of the Eastern Pamir, Western Pamir and Pamir Alay, hosts 249 surging glaciers and 128 surge-  
319 like glaciers. About 27.74% of the glacier area in the Eastern and Western Pamir belongs to surging glaciers. We also found  
320 28 surging tributaries in 15 glacier complexes in the Pamirs. Surging glaciers are also common in the Western Kunlun. In total  
321 82 surging and 47 surge-like glaciers were identified in the West Kunlun, and the area of surging glaciers accounted for 30.48%  
322 of the total glacier area. The Central Tien Shan has the fourth largest surging glacier area. In total 59 surging glaciers were  
323 identified in the Central Tien Shan, which covered 12.93% of the total glacier area. The Karakoram, Pamirs, West Kunlun,



324 and Central Tien Shan host ~83% of the surging glaciers across HMA. Figure 5 shows the distribution of identified surging  
325 and surge-like glaciers in these four regions.

326 Within interior HMA subregions (including the Tibetan Interior Mountains, Eastern Kunlun Shan, and Tanggula Shan), the  
327 number of identified surging glaciers represents less than 2% of the total but the area accounted for near 15% of the total  
328 glacial area. Surging glaciers in these regions are generally gathered in a few watersheds. Similar localized surging glacier  
329 clusters were also found in the Nyainqentanglha, Northern and Western Tien Shan, and Central Himalaya, but the  
330 corresponding area ratios are much lower. In these regions, our inventory covered dozens of surging glaciers which were rarely  
331 reported before. Figure 6 shows some samples of identified surging glaciers in these regions.

### 332 **5.3 Geometric characteristics of surging glaciers**

333 In this part, only the surging glaciers and non-surging- glaciers are taken for analysis. The surge-like glaciers are not included.  
334 All glacier samples in the surging and non-surging classes are larger than 0.40 km<sup>2</sup>.

335 We divided all glaciers into 9 classes according to their area, and calculated the ratios of surging glacier number and area in  
336 each class. As shown in Figure 7, surging glaciers were found in all classes. Both the ratios of surging glacier area and number  
337 became increasingly high as the glacier size increased, except for the last class. Surging glaciers with an area of 1~50 km<sup>2</sup>  
338 occupies 82% of all surging glaciers. For the three classes in which glaciers are larger than 50 km<sup>2</sup>, the ratios of surging glaciers  
339 area and number were about 52% and 54%, respectively. In particular, 2 of 6 very large glaciers (the Siachen glacier and  
340 Hispar glacier) surged during our observation periods.

341 When comparing the geometric characteristics of the surging glaciers and non-surging glaciers, we selected samples in the  
342 following way: for each surging glacier, we selected 10 non-surging glacier samples that have closest area; and then we  
343 randomly sampled 3 out of the 10 selected non-surging glaciers. This is to minimize the discrepancy resulted from the sample  
344 differences. There are two reasons for doing so. First, the gap between the sample numbers is huge (~35000 non-surging vs.  
345 890 surging). Second, a high proportion of non-surging glaciers are very small glaciers. The final selected 890×3 non-surging  
346 glaciers formed the reference group.

347 We first analysed the distribution of surging glacier number and area in eight orientations. As shown in Fig. 8, both the number  
348 and area of glaciers facing the north are the largest, and then followed by those facing the northwest and northeast. The  
349 distribution of the glacier orientation in reference group were different than that of the non-surging glaciers, which confirmed  
350 the statistical analysis would be affected by sample differences. The number of surging glaciers facing the north accounted for  
351 ~30.1% of the total surging glacier number, and their area accounted for ~27.8% of all surging glacier area. The number and  
352 area ratios of surging glaciers facing the north are obviously higher than that of the non-surging glaciers facing the north, while  
353 the number and area ratios of surging glaciers facing the northwest are obviously lower than that of the non-surging glaciers  
354 facing the northwest. Meanwhile, the area ratio of surging glaciers facing the northeast is considerable higher than the number  
355 ratio, but for surging glaciers facing the northwest and southwest the situation is opposite.

356 Figure 9 illustrates the comparisons between the basic geometric properties of surging and non-surging glaciers. The sampling  
357 strategy mention above was also utilized here. If we directly compare the surging glaciers with all non-surging glaciers, we  
358 will find that surging glaciers generally have a larger area, wider elevation range (i.e., the highest glacier surface elevation  
359 minus the lowest), and longer flowline (Fig 9a-c). Taking the median values as the candidates, the quantitative comparisons  
360 are 7.3 km<sup>2</sup> (surging) vs. 0.87 km<sup>2</sup> (non-surging) for glacier area, 1534 m vs. 642 m for elevation range, and 6695 m vs. 1854  
361 m for maximum glacier length, respectively. In terms of mean surface slope and median elevation, the values of the surging  
362 glaciers are less spread out than the non-surging glaciers. However, the median values of the two kinds of glaciers are very  
363 close (see Figures 9d and 9e). If we took the non-surging glaciers in reference group for comparisons, the discrepancies of two  
364 kinds of groups on these geometric properties became much more different. As shown in Figure 9a, the similar boxplots of  
365 reference group and surging glacier samples proved that our sampling strategy has successfully re-organized the non-surging

366 glacier samples for comparisons. The gaps between the surging and non-surging glaciers (reference group) in the glacier area  
367 ( $7.3 \text{ km}^2$  vs.  $7.0 \text{ km}^2$ ), elevation range (1534 m vs. 1180 m) and glacier length (6695 m vs. 5560 m), are much smaller. More  
368 importantly, the mean slope of the glaciers in reference group become smaller than that of the surging glaciers.  
369 The correlation between different glacier geometric properties was analysed through the bivariate scatterplots (see Figure 10).  
370 Among the glacier area, glacier length, and glacier surface elevation range, any two of them have an apparent positive  
371 correlation. The glacier mean slope has a moderate correlation with the glacier area, glacier length, and glacier elevation range.  
372 By contrast, the glacier median elevation has little correlation with glacier area, glacier length, glacier elevation range, and  
373 glacier mean slope. The correlation of any two geometric properties makes little difference between surging and non-surging  
374 glaciers.

## 375 **6 Discussion**

### 376 **6.1 Uncertainty analysis**

377 The reliability of surging glacier identification is directly related to the accuracy of glacier surface elevation change. Assuming  
378 the uncertainties in surface elevation change are similar over glacierized areas and stable areas, we evaluated the glacier  
379 elevation change uncertainties based on elevation change observations in stable areas, whose true values are zeros. Meanwhile,  
380 the uncertainties in the radar penetration calculation were also considered through the error propagation law. The normalized  
381 median absolute deviation (NMAD) is less sensitive to outliers and can be deemed as an alternative to standard deviation  
382 (Höhle and Höhle, 2009). Hence, the NMAD was used to denote the uncertainty of individual glacier surface elevation change  
383 tile (Li et al., 2017). Figure 11 shows the NMAD of elevation change observations in stable areas within each DEM  
384 differencing tile, which were used for the co-registration and biases removal during the glacier elevation change estimation.  
385 Due to large distortions in the KH-9 images, the NASADEM - KH-9 DEM results had the highest uncertainties. Benefiting  
386 from the advantages of bistatic SAR image pairs, the COP30 DEM has high quality, and the COP30 DEM related results had  
387 the lowest uncertainties. The HMA8m DEM related results had moderate uncertainties. The average NMAD of all DEM  
388 differencing tiles was smaller than 5 m. The significant elevation errors usually occurred in the highly rugged regions such as  
389 crests and horns. The terrain of glacier surface is relatively gentle, and therefore the uncertainties of glacier surface elevation  
390 changes should be lower than the estimated values over the area where surge occur. The top of glaciers usually includes very  
391 steep faces and have a lot of uncertainties, but it does not matter too much for this study. In general, the uncertainties of our  
392 elevation change results are well-controlled. Compared with the typical surface elevation change resulting from a glacier surge  
393 (tens to hundreds of meters), the magnitudes of uncertainties are very small.

394 Similar to previous studies (Sevestre and Benn, 2015; Goerlich et al., 2020), the surging glacier identification in this study  
395 was completed through a manual qualitative interpretation. It's difficult to provide a quantitative index to represent the  
396 uncertainty of surge identification. However, the four-class indicator of surge likelihood could aid that in a degree.

### 397 **6.2 Characteristics of surging glaciers**

398 The direct comparisons between geometric characteristics of surging and non-surging glaciers manifest that surge activity is  
399 more likely to occur in the glacier with a larger area, wider elevation range, and longer length (Fig. 9). Previous studies also  
400 reported this phenomenon (Barrand and Murray, 2006; Jiskoot, 2011; Sevestre and Benn, 2015; Mukherjee et al., 2017; Guillet  
401 et al., 2022). Larger area, wider elevation range, and longer length mean a larger glacier scale and more mass storage. Surge  
402 is a self-balancing process of a glacier to regulate its internal instability of thermal or hydrologic conditions which needs  
403 enough mass storage. In this case, about 97% of the surging glacier has an area larger than  $1 \text{ km}^2$ . For glaciers larger than  $10$   
404  $\text{km}^2$ , surge becomes a quite common behavior (with a number ratio higher than 20%), rather than an accidental behavior (see  
405 Fig.7).

406 In terms of mean surface slope, we could not observe a statistically difference in the median value of the surging and non-  
407 surging glaciers, although the surging glaciers have a more concentrated value range (Fig 9d and Figure 10, 3rd row, 1st  
408 column). After minimizing this kind of bias, we observed an obvious higher mean slope of surging glaciers in the comparison  
409 with the reference group. Several studies have demonstrated that the surging glacier tend to have shallower slope (Jiskoot et  
410 al., 2000; Guillet et al., 2022). However, here we reasonably argue that this rule was concluded from an unbalanced comparison,  
411 as non-surging glaciers have a higher proportion of small glaciers than surging glaciers. Meanwhile, the inverse relationship  
412 between the glacier slope and length (Clarke, 1991; Sevestre and Benn, 2015) may not apply to very small glaciers (i.e. smaller  
413 than 1 km<sup>2</sup>). As shown in Fig. 9d and Fig. 10, among the non-surging glaciers, the small ones occupy a high proportion and  
414 their mean slope presents strong variability. Regarding this, we can conclude that steeper glaciers are more likely to surge  
415 when the comparison is restricted to similar areas. As for the glacier median elevation, since it is almost irrelevant to the glacier  
416 area, glacier length, glacier elevation range, and glacier mean slope (see Fig. 10), it can be deemed as an irregular glacier index.  
417 However, among glaciers that have similar areas, steeper glaciers generally have lower median elevation. That's why the  
418 median elevation of surging glaciers is slightly smaller than that of non-surging glaciers (Fig. 9e).  
419 These comparisons could now lead to a conclusion as follows: the surging glaciers are generally longer, and have larger  
420 elevation range than non-surging glaciers, since they have more mass storage. However, when glaciers are similar in area, a  
421 steeper surface slope is more likely to lead to surge.

422 Besides, our results highlights that the ratio distribution of surging glaciers in eight aspects are slightly different from that of  
423 non-surging glaciers (see Fig. 8). Overall, the ratio of surging glaciers is relatively higher than the non-surging glaciers in the  
424 north and northeast directions, but lower in the northwest direction. It is generally known that glaciers facing the north are  
425 more developed in HMA. Due to the orientation of the mountains, most of the large glaciers flow toward the north and  
426 northeast. Besides, the area-to-number ratio of surging glaciers is much larger than non-surging glaciers in the northeast  
427 orientation, but smaller in the northwest orientation. This is true for the Karakoram, Pamirs, and West Kunlun Shan, the three  
428 largest clusters of surging glaciers, indicates that large northeast-facing glacier has higher possibility to be surging glacier.  
429 Accordingly, the surging glaciers facing the north and northeast have higher area ratio than that facing the northwest.

430 The spatial distribution of surging glaciers in HMA presents strong heterogeneity. About 83% of identified surging glaciers  
431 were located in the northwest region including the Central Tien Shan, Pamirs, Karakoram, and West Kunlun, and their area  
432 occupied about 87% of the total identified surging glacier area (see Fig. 4 and Table 2). As discussed above, larger glaciers  
433 are more likely to surge. The northwest regions generally hold more large glaciers, and therefore hold more surging glaciers.  
434 In other subregions, large glaciers are usually concentrated in some great ice fields, such as the Geladandong, Puruogangri,  
435 and Xinqingfeng. Accordingly, surging glaciers in these subregions are usually clustered in several watersheds.

436 Several studies have pointed out that glacier surge activities have little impact on the glacier mass balance (Gardelle et al.,  
437 2013; Bolch et al., 2017; Guillet et al., 2022). However, glacier mass balance may also affect the occurrence of glacier surge.  
438 Copland et al. (2011) concluded that the increase of glacier surges in the Karakoram could be related to the positive mass  
439 budget. The accumulated ice mass would accelerate a glacier to surge (Eisen et al., 2005; Kochtitzky et al., 2020), and the  
440 significant mass loss could prevent or postpone the surge in return (Dowdeswell et al., 1995). On a regional large scale, the  
441 relationship between mass balance and surge occurrence needs to be further analysed. Our glacier elevation change maps of  
442 the period 2000-2010s are similar to that derived by Brun et al. (2017) and Shean et al. (2020). We found that, at the regional  
443 scale, the occurrence of surging glaciers is correlated with the regional glacier mass balance. The three subregions holding the  
444 largest clusters of surging glaciers, i.e., the Pamirs, Karakoram, and West Kunlun, are characterized by slightly negative or  
445 positive mass budgets, which is known as the 'Pamir-Karakoram-West Kunlun' anomaly (Brun et al., 2017). Likewise, the  
446 subregions Central Tien Shan, Tibetan Interior Mountains, and East Kunlun Shan, which hold the moderate clusters of surging  
447 glaciers, have glacier mass loss rates much lower than the average rates of HMA. By contrast, subregions with severe glacier  
448 mass loss hold the lowest surging glacier ratio, such as the Dzhungarsky Alatau, Hengduan Shan, and Eastern Himalaya.

### 449 6.3 Comparison with previous surging glacier inventories

450 Guillet et al. (2022) presented a comprehensive surging glacier inventory of HMA for the period 2000-2018 from a multi-  
451 factor remote sensing approach. Prior to the comparison, we generated an inventory based on the RGI6.0, as Guillet et al.  
452 (2022) did. Guillet et al. (2022) identified 666 surging glaciers, and the area of surging glacier occupies 19.5% of the total  
453 glacier area. We identified 890 surging glaciers (809 if RGI6.0 was used), and their area only occupies 16.59% of the total  
454 glacier area. We attributed the lower area ratio of surging glaciers to two reasons. First, in our inventory the surging tributaries  
455 were separated from the non-surging trunks. Second, many outcrop rocks and shaded areas are excluded from the GAMDAM2  
456 glacier areas (Sakai, 2019), which would lower our surging area ratio, but make the result more accurate. If we assign our  
457 identified surging glaciers to the RGI6.0 polygons without tributary separation, the surging area ratio would be larger (20.25%).  
458 Within our inventory, 556 surging and 62 surge-like glaciers were also identified by Guillet et al. (2022), and the discrepancy  
459 of identifications mostly occurred on small glaciers. If only the period 2000-2020 was considered, 657 surging glaciers were  
460 identified by us, which is very close to that of Guillet et al. (665). For the period 1970s-2000, there are 151 surging and 101  
461 surge-like glaciers that were not identified by Guillet et al. (2022). Overall, we have newly identified 253 surging and 248  
462 surge-like glaciers. We owed the newly findings to the longer observation period and multiple elevation change observation.  
463 However, 47 surging glacier presented by Guillet et al. were missed in this study, and 62 surge-like glaciers in our new  
464 inventory were identified as surging glaciers by Guillet et al. (2022). We carefully checked the glaciers not included in our  
465 inventory but included in Guillet et al.'s inventory, as well as those included in our inventory but not included in Guillet et al.'s  
466 inventory, and this step helped us to find 21 more surging glaciers. We attribute this to the deficiency of using a single criterion,  
467 which could be aided by combining other features. Besides, the DEMs used in this study were suffering from the data voids  
468 and incomplete spatial coverage, especially for the KH-9 DEM, which could result in a relatively conservative identification.  
469 Multiple studies have identified surging glaciers in the Karakoram based on different data sources. For example, Bhambri et  
470 al. (2017) identified 221 surging and surge-like glaciers (the tributaries of a glacier system are counted as individual glaciers)  
471 based on the glacier morphology changes detected from spaceborne optical images acquired from 1972 to 2016, in-situ  
472 observations, and archive photos since the 1840s. However, the boundary used by Bhambri et al. (2017) to define the extent  
473 of Karakoram is much smaller than that used in our inventory. A much smaller group of surging glaciers (88) were identified  
474 by Copland et al. (2011) based on a similar method and the data acquired between 1960 and 2013. Rankl et al. (2014) identified  
475 101 surging glaciers in the Karakoram by detecting the changes in glacier surface velocity and terminus position between 1976  
476 and 2012. The results of Guillet et al. (2022) should be more reliable than previous ones, because more criteria were used for  
477 identifying surging glaciers. Compared with previous inventories, our inventory includes more surging glaciers (354). Among  
478 the 223 surging glaciers in the Karakoram identified by Guillet et al. (2022), 203 were identified as surging glaciers, and 12  
479 were identified as surge-like glaciers in this study, which means only 8 surging glaciers presented by Guillet et al. (2022) were  
480 not included in our inventory. The high coincidence between the two inventories indicates our surging glacier identification  
481 result is reliable. In total, we have newly identified 101 surging and 101 surge-like glaciers in this region.

482 Based on the method of glacier terminus change monitoring in Google Earth Engine, Vale et al. (2021) identified obvious  
483 terminus change of 137 surging glaciers. We found 127 verified surging and 6 surge-like glaciers in our inventory were  
484 included in their inventory, i.e., only four glaciers were missed in this study. The possible reason for this gap is that the  
485 technique used by Vale et al. cannot identify the internal glacier surges than did not cause terminus advancing. Also, the  
486 inadequate quality and spatial resolution of satellite images could limit the performance of detecting changes in glacier  
487 terminus position.

488 In the Pamirs, Sevestre and Been (2015) identified 820 surge-type glaciers based on publications and reports, but Goerlich et  
489 al. (2020) reported only 186 surging glaciers based on the observations of glacier flow velocity, elevation change, etc.. We  
490 found that, if Goerlich et al. (2020) applied the GAMDAM2 glacier polygons used in this study, the number of identified  
491 surging glaciers should be 182. Among the 182 surging glaciers identified by Goerlich et al. (2020), 153 and 15 were identified

492 as surging and surge-like glaciers in our study, respectively. Although 14 surging glaciers are missed in this study, our  
493 inventory has contained other 94 surging and 44 surge-like glaciers. The main cause for the result discrepancy is that the glacier  
494 elevation change observation conducted by Goerlich et al. (2020) only covered parts of the Western Pamir and only the  
495 observations before 2000 were used. In this region our inventory shared 193 surging glaciers with Guillet et al.'s inventory,  
496 and 185 of them were identified during the period 2000-2020, which also manifests a high coincidence of the two results.  
497 In the West Kunlun, Yasuda and Furuya (2015) reported 9 surging glaciers in the main range only, based on changes in glacier  
498 flow velocity and terminus position of 31 glaciers, and other 9 surging glaciers were found in the northwest part of the West  
499 Kunlun Shan by Chudley et al. (2019). A larger number (60) were found by Guillet et al. (2022). However, our inventory has  
500 even included more surging (82) and surge-like (47) glaciers in the West Kunlun Shan. During the period 2000-2020, we have  
501 identified 61 surging glaciers, which is very close to the number presented by Guillet et al. (2022). In Central Tien Shan,  
502 Mukherjee et al. (2017) identified 39 surge-type (including 9 surging and 13 very probable surging) glaciers through the  
503 analysis of changes in surface elevation and morphology from 1964 to 2014, whereas 79 (59 surging and 20 surge-like) were  
504 identified in our studies. The insufficient coverage of elevation change observation (only covered the west part of the Central  
505 Tien Shan) may be the main reason for the discrepancy in identification results. Guillet et al. (2022) identified 54 surging  
506 glaciers during 2000-2018, in which 36 were confirmed in our inventory.

## 507 **7 Conclusions**

508 This study presented a new inventory of surging glaciers across the entire HMA range, which was accomplished based on the  
509 glacier surface elevation changes derived from multiple elevation sources, by using the morphological changes from optical  
510 images as complements. In total 890 surging and 336 surge-like glaciers were identified in the new inventory. Through the  
511 analysis of geometric parameters, we found that surging glaciers generally have a greater area, length, and elevation range than  
512 non-surging glaciers. However, the differences are smaller if taking the glacier size distribution into account. When considering  
513 glaciers of similar area, the steeper ones are more likely to surge. Furthermore, combining the region-wide glacier mass balance  
514 measurements, we found a similar distribution between the positive mass balance and number of surging glaciers. Benefiting  
515 from the long period and wide coverage of surface elevation change observations, our study newly identified 253 surging and  
516 248 surge-like glaciers in HMA than previous inventory (Guillet et al., 2022). However, our inventory does not provide the  
517 surge duration period and the maximum flow velocity to describe the dynamic process of each glacier surge activity.  
518 Improvements should be made by combining multi-criteria identification methods. Considering the fact that glacier surges are  
519 more widespread than we thought, the inventory presented in this study still needs further replenishment.

## 520 **8 Data and code availability**

521 The presented inventory and corresponding multi-temporal elevation change results of identified surging glaciers are freely  
522 available at: <https://doi.org/10.5281/zenodo.7590838> (Guo et al., 2022). The inventory is distributed in the format of  
523 GeoPackage (.gpkg) and ESRI shpfile (.shp), which is represented by outline or manually defined center point of surging  
524 glaciers with geometric attributes. The glacier polygons of the inventory are compiled from the GAMDAM2 glacier inventory.  
525 In total eight fields are integrated in the attributes table to describe the surging information of corresponding glacier as  
526 mentioned in section 4.3. The description of each field in the attribute table is listed in Table 3. The DEM differencing results  
527 of COP30 DEM - NASADEM, HMA8m DEM - NASADEM, and NASADEM - KH-9 DEM are compressed into individual  
528 zip file, respectively. The elevation change results of surging glaciers were divided into multi-temporal  $1^\circ \times 1^\circ$  tiled GeoTiff  
529 grids. The metadata file is stored in a text file (README.txt), which contains the datasets description and details of the attribute  
530 information of the inventory.

531 The code used for elevation change estimation can be available at: [https://github.com/TristanBlus/dem\\_coreg](https://github.com/TristanBlus/dem_coreg). This code was  
532 developed based on the *demcoreg* package (Shean et al., 2019).

### 533 **Author contribution**

534 J.L. and L.G. conceived this study and wrote the paper. L.G. developed the processing flow, compiled the inventory and drew  
535 the figures with the support from J.L. A.D. generated the KH-9 DEM. A.D., Z.L. and X.L. helped with the results analysis and  
536 discussions and manuscript editing. Z.L., J.L. and J.Z. provided the funding acquisition. All authors have contributed and  
537 agreed to the published version of the manuscript.

### 538 **Competing interest**

539 The authors declare that they have no conflict of interest.

### 540 **Acknowledgments**

541 The authors express gratitude to all institution that provide us the opensource dataset used in this study: the NASADEM from  
542 LP DAAC ([https://e4ftl01.cr.usgs.gov/MEASURES/NASADEM\\_HGT.001/](https://e4ftl01.cr.usgs.gov/MEASURES/NASADEM_HGT.001/)), the Copernicus DEM from European Space  
543 Agency (ESA) (<https://spacedata.copernicus.eu/web/cscda/cop-dem-faq>), the HMA8m DEM processed by David Shean from  
544 National Snow and Ice Data Center (NSIDC) ([https://nsidc.org/data/HMA\\_DEM8m\\_MOS/versions/1](https://nsidc.org/data/HMA_DEM8m_MOS/versions/1)), and the Randolph  
545 Glacier Inventory Version 6.0 (<http://www.glims.org/RGI/randolph.html>). The authors also appreciate the valuable comments  
546 from Frank Pual and Guillet Gregoire.

### 547 **Financial support**

548 This work was supported by the National Natural Science Fund for Distinguished Young Scholars (41925016), the Strategic  
549 Priority Research Program of Chinese Academy of Sciences (XDA20100101), the National Natural Science Foundation of  
550 China (41904006), the Hunan Key Laboratory of remote sensing of ecological environment in Dongting Lake Area (No. 2021-  
551 010), the Fundamental Research Funds for the Central Universities of Central South University (2021zzts0265).

### 552 **References**

- 553 Abdel Jaber, W., Rott, H., Floricioiu, D., Wuite, J., and Miranda, N.: Heterogeneous spatial and temporal pattern of surface  
554 elevation change and mass balance of the Patagonian ice fields between 2000 and 2016, *The Cryosphere*, 13, 2511–2535,  
555 doi:10.5194/tc-13-2511-2019, 2019.
- 556 AIRBUS: Copernicus Digital Elevation Model Validation Report, AIRBUS Defence and Space GmbH, 2020.
- 557 An, B., Wang, W., Yang, W., Wu, G., Guo, Y., Zhu, H., Gao, Y., Bai, L., Zhang, F., Zeng, C., Wang, L., Zhou, J., Li, X., Li,  
558 J., Zhao, Z., Chen, Y., Liu, J., Li, J., Wang, Z., Chen, W., and Yao, T.: Process, mechanisms, and early warning of glacier  
559 collapse-induced river blocking disasters in the Yarlung Tsangpo Grand Canyon, southeastern Tibetan Plateau, *Sci. Total*  
560 *Environ.*, 151652, doi:10.1016/j.scitotenv.2021.151652, 2021.
- 561 Barrand, N. E. and Murray, T.: Multivariate Controls on the Incidence of Glacier Surging in the Karakoram Himalaya, *Arct.*  
562 *Antarct. Alp. Res.*, 38, 489–498, doi:10.1657/1523-0430(2006)38[489:MCOTIO]2.0.CO;2, 2006.

563 Beaud, F., Aati, S., Delaney, I., Adhikari, S., and Avouac, J.-P.: Generalized sliding law applied to the surge dynamics of  
564 Shisper Glacier and constrained by timeseries correlation of optical satellite images, *Glaciers/Remote Sensing*, doi:10.5194/tc-  
565 2021-96, 2021.

566 Benn, D. I., Fowler, A. C., Hewitt, I., and Sevestre, H.: A general theory of glacier surges, *J. Glaciol.*, 65, 701–716,  
567 doi:10.1017/jog.2019.62, 2019.

568 Bhambri, R., Hewitt, K., Kawishwar, P., and Pratap, B.: Surge-type and surge-modified glaciers in the Karakoram, *Sci. Rep.*,  
569 7, doi:10.1038/s41598-017-15473-8, 2017.

570 Bhambri, R., Hewitt, K., Haritashya, U. K., Chand, P., Kumar, A., Verma, A., Tiwari, S. K., and Rai, S. K.: Characteristics of  
571 surge-type tributary glaciers, Karakoram, *Geomorphology*, 403, 108161, doi:10.1016/j.geomorph.2022.108161, 2022.

572 Bolch, T., Kulkarni, A., Kaab, A., Huggel, C., Paul, F., Cogley, J. G., Frey, H., Kargel, J. S., Fujita, K., Scheel, M., Bajracharya,  
573 S., and Stoffel, M.: The State and Fate of Himalayan Glaciers, *Science*, 336, 310–314, doi:10.1126/science.1215828, 2012.

574 Bolch, T., Pieczonka, T., Mukherjee, K., and Shea, J.: Brief communication: Glaciers in the Hunza catchment (Karakoram)  
575 have been nearly in balance since the 1970s, *The Cryosphere*, 11, 531–539, doi:10.5194/tc-11-531-2017, 2017.

576 Bolch, T., Shea, J. M., Liu, S., Azam, F. M., Gao, Y., Gruber, S., Immerzeel, W. W., Kulkarni, A., Li, H., Tahir, A. A., Zhang,  
577 G., and Zhang, Y.: Status and Change of the Cryosphere in the Extended Hindu Kush Himalaya Region, in: *The Hindu Kush  
578 Himalaya Assessment*, edited by: Wester, P., Mishra, A., Mukherji, A., and Shrestha, A. B., Springer International Publishing,  
579 Cham, 209–255, doi:10.1007/978-3-319-92288-1\_7, 2019.

580 Brun, F., Berthier, E., Wagnon, P., Kääb, A., and Treichler, D.: A spatially resolved estimate of High Mountain Asia glacier  
581 mass balances from 2000 to 2016, *Nat. Geosci.*, 10, 668–673, doi:10.1038/ngeo2999, 2017.

582 Chudley, T. R. and Willis, I. C.: Glacier surges in the north-west West Kunlun Shan inferred from 1972 to 2017 Landsat  
583 imagery, *J. Glaciol.*, 65, 1–12, doi:10.1017/jog.2018.94, 2019.

584 Clarke, G. K. C.: Length, width and slope influences on glacier surging, *J. Glaciol.*, 37, 236–246,  
585 doi:10.3189/S0022143000007255, 1991.

586 Clarke, G. K. C., Schmok, J. P., Ommanney, C. S. L., and Collins, S. G.: Characteristics of surge-type glaciers, *J. Geophys.  
587 Res. Solid Earth*, 91, 7165–7180, doi:10.1029/JB091iB07p07165, 1986.

588 Cogley, J. G., Arendt, A. A., Bauder, A., Braithwaite, R. J., Hock, R., J. B., R., Jansson, P., Kaser, G., Moller, M., Nicholson,  
589 L., Rasmussen, L. A., and Zemp, M.: Glossary of glacier mass balance and related terms, IACS Contribution No.2, UNESCO,  
590 Paris, 2011.

591 Copland, L., Sylvestre, T., Bishop, M. P., Shroder, J. F., Seong, Y. B., Owen, L. A., Bush, A., and Kamp, U.: Expanded and  
592 Recently Increased Glacier Surging in the Karakoram, *Arct. Antarct. Alp. Res.*, 43, 503–516, 2011.

593 Crippen, R., Buckley, S., Agram, P., Belz, E., Gurrola, E., Hensley, S., Kobrick, M., Lavallo, M., Martin, J., Neumann, M.,  
594 Nguyen, Q., Rosen, P., Shimada, J., Simard, M., and Tung, W.: NASADEM global elevation model: methods and progress,  
595 *ISPRS - Int. Arch. Photogramm. Remote Sens. Spat. Inf. Sci.*, XLI-B4, 125–128, doi:10.5194/isprsarchives-XLI-B4-125-2016,  
596 2016.

597 Dehecq, A., Gardner, A. S., Alexandrov, O., McMichael, S., Hugonnet, R., Shean, D., and Marty, M.: Automated Processing  
598 of Declassified KH-9 Hexagon Satellite Images for Global Elevation Change Analysis Since the 1970s, *Front. Earth Sci.*, 8,  
599 566802, doi:10.3389/feart.2020.566802, 2020.

600 Dowdeswell, J. A., Hodgkins, R., Nuttall, A.-M., Hagen, J. O., and Hamilton, G. S.: Mass balance change as a control on the  
601 frequency and occurrence of glacier surges in Svalbard, Norwegian High Arctic, *Geophys. Res. Lett.*, 22, 2909–2912,  
602 doi:10.1029/95GL02821, 1995.

603 Eisen, O., Harrison, W. D., Raymond, C. F., Echelmeyer, K. A., Bender, G. A., and Gorda, J. L. D.: Variegated Glacier, Alaska,  
604 USA: a century of surges, *J. Glaciol.*, 51, 399–406, doi:10.3189/172756505781829250, 2005.

605 Fan, Y., Ke, C.-Q., Zhou, X., Shen, X., Yu, X., and Lhakpa, D.: Glacier mass-balance estimates over High Mountain Asia  
606 from 2000 to 2021 based on ICESat-2 and NASADEM, *J. Glaciol.*, 1–13, doi:10.1017/jog.2022.78, 2022.

607 Farinotti, D., Immerzeel, W. W., Kok, R., Quincey, D. J., and Dehecq, A.: Manifestations and mechanisms of the Karakoram  
608 glacier Anomaly, *Nat. Geosci.*, 13, 8–16, doi:10.1038/s41561-019-0513-5, 2020.

609 Farnsworth, W. R., Ingólfsson, Ó., Retelle, M., and Schomacker, A.: Over 400 previously undocumented Svalbard surge-type  
610 glaciers identified, *Geomorphology*, 264, 52–60, doi:10.1016/j.geomorph.2016.03.025, 2016.

611 Farr, T. G., Rosen, P. A., Caro, E., Crippen, R., Duren, R., Hensley, S., Kobrick, M., Paller, M., Rodriguez, E., Roth, L., Seal,  
612 D., Shaffer, S., Shimada, J., Umland, J., Werner, M., Oskin, M., Burbank, D., and Alsdorf, D.: The Shuttle Radar Topography  
613 Mission, *Rev. Geophys.*, 45, RG2004, doi:10.1029/2005RG000183, 2007.

614 Fowler, A. C.: A theory of glacier surges, *J. Geophys. Res.*, 92, 9111, doi:10.1029/JB092iB09p09111, 1987.

615 Fowler, A. C., Murray, T., and Ng, F. S. L.: Thermally controlled glacier surging, *J. Glaciol.*, 47, 527–538,  
616 doi:10.3189/172756501781831792, 2001.

617 Gardelle, J., Berthier, E., Arnaud, Y., and Käab, A.: Region-wide glacier mass balances over the Pamir-Karakoram-Himalaya  
618 during 1999–2011, *Cryosphere Discuss.*, 7, 975–1028, doi:10.5194/tcd-7-975-2013, 2013.

619 Goerlich, F., Bolch, T., and Paul, F.: More dynamic than expected: an updated survey of surging glaciers in the Pamir, *Earth  
620 Syst. Sci. Data*, 12, 3161–3176, doi:10.5194/essd-12-3161-2020, 2020.

621 Guillet, G., King, O., Lv, M., Ghuffar, S., Benn, D., Quincey, D., and Bolch, T.: A regionally resolved inventory of High  
622 Mountain Asia surge-type glaciers, derived from a multi-factor remote sensing approach, *The Cryosphere*, 16, 603–623,  
623 doi:10.5194/tc-16-603-2022, 2022.

624 Guth, P. L. and Geoffroy, T. M.: LiDAR point cloud and ICESat-2 evaluation of 1 second global digital elevation models:  
625 Copernicus wins, *Trans. GIS*, 25, 2245–2261, doi:10.1111/tgis.12825, 2021.

626 Hewitt, K.: The Karakoram Anomaly? Glacier Expansion and the ‘Elevation Effect,’ *Karakoram Himalaya, Mt. Res. Dev.*, 25,  
627 332–340, doi:10.1659/0276-4741(2005)025[0332:TKAGEA]2.0.CO;2, 2005.

628 Hewitt, K.: Tributary glacier surges: an exceptional concentration at Panmah Glacier, Karakoram Himalaya, *J. Glaciol.*, 53,  
629 181–188, doi:10.3189/172756507782202829, 2007.

630 Höhle, J. and Höhle, M.: Accuracy assessment of digital elevation models by means of robust statistical methods, *ISPRS J.  
631 Photogramm. Remote Sens.*, 64, 398–406, doi:10.1016/j.isprsjprs.2009.02.003, 2009.

632 Holzer, N., Vijay, S., Yao, T., Xu, B., Buchroithner, M., and Bolch, T.: Four decades of glacier variations at Muztagh Ata  
633 (eastern Pamir): a multi-sensor study including Hexagon KH-9 and Pléiades data, *The Cryosphere*, 9, 2071–2088,  
634 doi:10.5194/tc-9-2071-2015, 2015.

635 Hugonnet, R., McNabb, R., Berthier, E., Menounos, B., Nuth, C., Girod, L., Farinotti, D., Huss, M., Dussailant, I., Brun, F.,  
636 and Käab, A.: Accelerated global glacier mass loss in the early twenty-first century, *Nature*, 592, 726–731,  
637 doi:10.1038/s41586-021-03436-z, 2021.

638 Jacquemart, M. and Cicoira, A.: Hazardous Glacier Instabilities: Ice Avalanches, Sudden Large-Volume Detachments of Low-  
639 Angle Mountain Glaciers, and Glacier Surges, in: *Treatise on Geomorphology*, Elsevier, 330–345, doi:10.1016/B978-0-12-  
640 818234-5.00188-7, 2022.

641 Jiskoot, H.: Glacier Surging, in: *Encyclopedia of Snow, Ice and Glaciers*, edited by: Singh, V. P., Singh, P., and Haritashya,  
642 U. K., Springer Netherlands, Dordrecht, 415–428, doi:10.1007/978-90-481-2642-2\_559, 2011.

643 Jiskoot, H., Murray, T., and Boyle, P.: Controls on the distribution of surge-type glaciers in Svalbard, *J. Glaciol.*, 46, 412–422,  
644 doi:10.3189/172756500781833115, 2000.

645 Käab, A., Leinss, S., Gilbert, A., Bühler, Y., Gascoïn, S., Evans, S. G., Bartelt, P., Berthier, E., Brun, F., Chao, W.-A., Farinotti,  
646 D., Gimbert, F., Guo, W., Huggel, C., Kargel, J. S., Leonard, G. J., Tian, L., Treichler, D., and Yao, T.: Massive collapse of



647 two glaciers in western Tibet in 2016 after surge-like instability, *Nat. Geosci.*, 11, 114–120, doi:10.1038/s41561-017-0039-7,  
648 2018.

649 Kääb, A., Jacquemart, M., Gilbert, A., Leinss, S., Girod, L., Huggel, C., Falaschi, D., Ugalde, F., Petrakov, D., Chernomorets,  
650 S., Dokukin, M., Paul, F., Gascoïn, S., Berthier, E., and Kargel, J. S.: Sudden large-volume detachments of low-angle mountain  
651 glaciers – more frequent than thought?, *The Cryosphere*, 15, 1751–1785, doi:10.5194/tc-15-1751-2021, 2021.

652 Kamb, B.: Glacier surge mechanism based on linked cavity configuration of the basal water conduit system, *J. Geophys. Res.*,  
653 92, 9083, doi:10.1029/JB092iB09p09083, 1987.

654 Kochtitzky, W., Winski, D., McConnell, E., Kreutz, K., Campbell, S., Enderlin, E. M., Copland, L., Williamson, S., Main, B.,  
655 and Jiskoot, H.: Climate and surging of Donjek Glacier, Yukon, Canada, *Arct. Antarct. Alp. Res.*, 52, 264–280,  
656 doi:10.1080/15230430.2020.1744397, 2020.

657 Li, J., Li, Z., Zhu, J., Li, X., Xu, B., Wang, Q., Huang, C., and Hu, J.: Early 21st century glacier thickness changes in the  
658 Central Tien Shan, *Remote Sens. Environ.*, 192, 12–29, doi:10.1016/j.rse.2017.02.003, 2017.

659 Lv, M., Guo, H., Lu, X., Liu, G., Yan, S., Ruan, Z., Ding, Y., and Quincey, D. J.: Characterizing the behaviour of surge- and  
660 non-surge-type glaciers in the Kingata Mountains, eastern Pamir, from 1999 to 2016, *The Cryosphere*, 13, 219–236,  
661 doi:10.5194/tc-13-219-2019, 2019.

662 Lv, M., Guo, H., Yan, J., Wu, K., Liu, G., Lu, X., Ruan, Z., and Yan, S.: Distinguishing Glaciers between Surging and  
663 Advancing by Remote Sensing: A Case Study in the Eastern Karakoram, *Remote Sens.*, 12, 2297, doi:10.3390/rs12142297,  
664 2020.

665 Maurer, J. M., Schaefer, J. M., Rupper, S., and Corley, A.: Acceleration of ice loss across the Himalayas over the past 40 years,  
666 *Sci. Adv.*, 5, eaav7266, doi:10.1126/sciadv.aav7266, 2019.

667 Maussion, F., Scherer, D., Mölg, T., Collier, E., Curio, J., and Finkelnburg, R.: Precipitation Seasonality and Variability over  
668 the Tibetan Plateau as Resolved by the High Asia Reanalysis, *J. Clim.*, 27, 1910–1927, doi:10.1175/JCLI-D-13-00282.1, 2014.

669 Maussion, F., Butenko, A., Champollion, N., Dusch, M., Eis, J., Fourteau, K., Gregor, P., Jarosch, A. H., Landmann, J.,  
670 Oesterle, F., Recinos, B., Rothenpieler, T., Vlug, A., Wild, C. T., and Marzeion, B.: The Open Global Glacier Model (OGGM)  
671 v1.1, *Geosci. Model Dev.*, 12, 909–931, doi:10.5194/gmd-12-909-2019, 2019.

672 Muhammad, S., Li, J., Steiner, J. F., Shrestha, F., Shah, G. M., Berthier, E., Guo, L., Wu, L., and Tian, L.: A holistic view of  
673 Shisper Glacier surge and outburst floods: from physical processes to downstream impacts, *Geomat. Nat. Hazards Risk*, 12,  
674 2755–2775, doi:10.1080/19475705.2021.1975833, 2021.

675 Mukherjee, K., Bolch, T., Goerlich, F., Kutuzov, S., Osmonov, A., Pieczonka, T., and Shesterova, I.: Surge-Type Glaciers in  
676 the Tien Shan (Central Asia), *Arct. Antarct. Alp. Res.*, 49, 147–171, doi:10.1657/AAAR0016-021, 2017.

677 Murray, T., Strozzi, T., Luckman, A., Jiskoot, H., and Christakos, P.: Is there a single surge mechanism? Contrasts in dynamics  
678 between glacier surges in Svalbard and other regions: IS THERE A SINGLE SURGE MECHANISM?, *J. Geophys. Res. Solid*  
679 *Earth*, 108, doi:10.1029/2002JB001906, 2003.

680 Nuimura, T., Sakai, A., Taniguchi, K., Nagai, H., Lamsal, D., Tsutaki, S., Kozawa, A., Hoshina, Y., Takenaka, S., Omiya, S.,  
681 Tsunematsu, K., Tshering, P., and Fujita, K.: The GAMDAM glacier inventory: a quality-controlled inventory of Asian  
682 glaciers, *The Cryosphere*, 9, 849–864, doi:10.5194/tc-9-849-2015, 2015.

683 Nuth, C. and Kääb, A.: Co-registration and bias corrections of satellite elevation data sets for quantifying glacier thickness  
684 change, *The Cryosphere*, 5, 271–290, doi:10.5194/tc-5-271-2011, 2011.

685 Paul, F.: Revealing glacier flow and surge dynamics from animated satellite image sequences: examples from the Karakoram,  
686 *The Cryosphere*, 9, 2201–2214, doi:10.5194/tc-9-2201-2015, 2015.

687 Paul, F.: Repeat Glacier Collapses and Surges in the Amney Machen Mountain Range, Tibet, Possibly Triggered by a  
688 Developing Rock-Slope Instability, *Remote Sens.*, 11, 708, doi:10.3390/rs11060708, 2019.

689 Purinton, B. and Bookhagen, B.: Beyond Vertical Point Accuracy: Assessing Inter-pixel Consistency in 30 m Global DEMs  
690 for the Arid Central Andes, *Front. Earth Sci.*, 9, 758606, doi:10.3389/feart.2021.758606, 2021.

691 Quincey, D. J., Braun, M., Glasser, N. F., Bishop, M. P., Hewitt, K., and Luckman, A.: Karakoram glacier surge dynamics,  
692 *Geophys. Res. Lett.*, 38, n/a-n/a, doi:10.1029/2011GL049004, 2011.

693 Rankl, M., Kienholz, C., and Braun, M.: Glacier changes in the Karakoram region mapped by multitemporal satellite imagery,  
694 *The Cryosphere*, 8, 977–989, doi:10.5194/tc-8-977-2014, 2014.

695 Round, V., Leinss, S., Huss, M., Haemmig, C., and Hajnsek, I.: Surge dynamics and lake outbursts of Kyagar Glacier,  
696 Karakoram, *The Cryosphere*, 11, 723–739, doi:10.5194/tc-11-723-2017, 2017.

697 Sakai, A.: Brief communication: Updated GAMDAM glacier inventory over high-mountain Asia, *The Cryosphere*, 13, 2043–  
698 2049, doi:10.5194/tc-13-2043-2019, 2019.

699 Sevestre, H. and Benn, D. I.: Climatic and geometric controls on the global distribution of surge-type glaciers: implications  
700 for a unifying model of surging, *J. Glaciol.*, 61, 646–662, doi:10.3189/2015JoG14J136, 2015.

701 Shean, D., Shashank Bhushan, Lilien, D., and Meyer, J.: dshean/demcoreg: Zenodo DOI release, ,  
702 doi:10.5281/ZENODO.3243481, 2019.

703 Shean, D. E., Alexandrov, O., Moratto, Z. M., Smith, B. E., Joughin, I. R., Porter, C., and Morin, P.: An automated, open-  
704 source pipeline for mass production of digital elevation models (DEMs) from very-high-resolution commercial stereo satellite  
705 imagery, *ISPRS J. Photogramm. Remote Sens.*, 116, 101–117, doi:10.1016/j.isprsjprs.2016.03.012, 2016.

706 Shean, D. E., Bhushan, S., Montesano, P., Rounce, D. R., Arendt, A., and Osmanoglu, B.: A Systematic, Regional Assessment  
707 of High Mountain Asia Glacier Mass Balance, *Front. Earth Sci.*, 7, 363, doi:10.3389/feart.2019.00363, 2020.

708 Shugar, D. H., Jacquemart, M., Shean, D., Bhushan, S., Upadhyay, K., Sattar, A., Schwanghart, W., McBride, S., de Vries, M.  
709 V. W., Mergili, M., Emmer, A., Deschamps-Berger, C., McDonnell, M., Bhambri, R., Allen, S., Berthier, E., Carrivick, J. L.,  
710 Clague, J. J., Dokukin, M., Dunning, S. A., Frey, H., Gascoïn, S., Haritashya, U. K., Huggel, C., Käab, A., Kargel, J. S.,  
711 Kavanaugh, J. L., Lacroix, P., Petley, D., Rupper, S., Azam, M. F., Cook, S. J., Dimri, A. P., Eriksson, M., Farinotti, D., Fiddes,  
712 J., Gnyawali, K. R., Harrison, S., Jha, M., Koppes, M., Kumar, A., Leinss, S., Majeed, U., Mal, S., Muhuri, A., Noetzi, J.,  
713 Paul, F., Rashid, I., Sain, K., Steiner, J., Ugalde, F., Watson, C. S., and Westoby, M. J.: A massive rock and ice avalanche  
714 caused the 2021 disaster at Chamoli, Indian Himalaya, *Science*, 373, 300–306, doi:10.1126/science.abh4455, 2021.

715 Steiner, J. F., Kraaijenbrink, P. D. A., Jiduc, S. G., and Immerzeel, W. W.: Brief communication: The Khurdopin glacier surge  
716 revisited – extreme flow velocities and formation of a dammed lake in 2017, *The Cryosphere*, 12, 95–101, doi:10.5194/tc-12-  
717 95-2018, 2018.

718 Surazakov, A. and Aizen, V.: Positional Accuracy Evaluation of Declassified Hexagon KH-9 Mapping Camera Imagery,  
719 *Photogramm. Eng. Remote Sens.*, 76, 603–608, doi:10.14358/PERS.76.5.603, 2010.

720 Thøgersen, K., Gilbert, A., Schuler, T. V., and Malthé-Sørensen, A.: Rate-and-state friction explains glacier surge propagation,  
721 *Nat. Commun.*, 10, 2823, doi:10.1038/s41467-019-10506-4, 2019.

722 Vale, A. B., Arnold, N. S., Rees, W. G., and Lea, J. M.: Remote Detection of Surge-Related Glacier Terminus Change across  
723 High Mountain Asia, *Remote Sens.*, 13, 1309, doi:10.3390/rs13071309, 2021.

724 Van Wyk de Vries, M., Wickert, A. D., MacGregor, K. R., Rada, C., and Willis, M. J.: Atypical landslide induces speedup,  
725 advance, and long-term slowdown of a tidewater glacier, *Geology*, doi:10.1130/G49854.1, 2022.

726 Yamazaki, D., Ikeshima, D., Tawatari, R., Yamaguchi, T., O’Loughlin, F., Neal, J. C., Sampson, C. C., Kanae, S., and Bates,  
727 P. D.: A high-accuracy map of global terrain elevations, *Geophys. Res. Lett.*, 44, 5844–5853, doi:10.1002/2017GL072874,  
728 2017.

729 Yasuda, T. and Furuya, M.: Dynamics of surge-type glaciers in West Kunlun Shan, Northwestern Tibet: SURGE-TYPE  
730 GLACIERS IN WEST KUNLUN SHAN, *J. Geophys. Res. Earth Surf.*, 120, 2393–2405, doi:10.1002/2015JF003511, 2015.

- 731 Zhou, S., Yao, X., Zhang, D., Zhang, Y., Liu, S., and Min, Y.: Remote Sensing Monitoring of Advancing and Surging Glaciers  
 732 in the Tien Shan, 1990–2019, *Remote Sens.*, 13, 1973, doi:10.3390/rs13101973, 2021.
- 733 Zhou, Y., Li, Z., and Li, J.: Slight glacier mass loss in the Karakoram region during the 1970s to 2000 revealed by KH-9  
 734 images and SRTM DEM, *J. Glaciol.*, 63, 331–342, doi:10.1017/jog.2016.142, 2017.
- 735 Zhou, Y., Li, Z., Li, J., Zhao, R., and Ding, X.: Glacier mass balance in the Qinghai–Tibet Plateau and its surroundings from  
 736 the mid-1970s to 2000 based on Hexagon KH-9 and SRTM DEMs, *Remote Sens. Environ.*, 210, 96–112,  
 737 doi:10.1016/j.rse.2018.03.020, 2018.

738 **Tables and Figures**

739 **Table 1: Surging glacier identification results**

Glacier changes	Identification class			Total
	I	II	III	
2000-2020 elevation change	719	157	169	1045
1970s-2000 elevation change	507	156	57	720
1986-2021 terminus advance	247	397	-	645
1986-2021 looped moraine	112	31	-	144
1986-2021 medial moraine	69	29	-	108
<b>Final identified surging glaciers</b>	890 (verified)	208 (probable)	128 (possible)	1226

740 **Table 2: Results of surging glacier identification in 22 subregions of HMA. Only glaciers larger than 0.4 km<sup>2</sup> were considered in the**  
 741 **glacier number related values.**

HiMAP regions	Glacier Number				Glacier Area			
	Surging	Surge-like	Total	Ratio (%)	Surging	Surge-like	Total	Ratio (%)
Karakoram	354	128	4121	8.59	7936.12	1329.40	20103.68	39.48
Western Pamir	188	48	3058	6.15	2232.52	289.597	8172.64	27.32
Western Kunlun Shan	82	47	2508	3.27	2580.21	589.17	8466.12	30.48
Central Tien Shan	59	20	2248	2.62	881.61	305.47	6816.95	12.93
Eastern Pamir	56	16	1148	4.88	796.35	79.12	2746.47	29.00
Tanggula Shan	22	4	697	3.16	441.94	41.71	1937.39	22.81
Tibetan Interior Mountains	22	12	1471	1.50	286.29	140.22	3933.48	7.28
Northern Western Tien Shan	21	6	1374	1.53	116.27	81.09	2502.60	4.65
Central Himalaya	17	21	3433	0.50	164.12	185.07	9928.72	1.65
Eastern Kunlun Shan	16	7	1191	1.34	458.11	55.38	2960.26	15.48
Nyainqentanglha	10	5	2916	0.34	119.53	184.79	7216.62	1.66
Eastern Hindu Kush	9	5	1279	0.70	178.18	77.19	3055.80	5.83
Western Himalaya	9	4	3659	0.25	110.22	69.41	8619.19	1.28
Eastern Himalaya	6	0	1334	0.45	94	0	3371.89	2.79
Pamir Alay	5	0	991	0.50	35.72	0	1957.94	1.82
Qilian Shan	4	6	851	0.47	35.99	26.40	1627.94	2.21
Eastern Tibetan Mountains	3	2	156	1.92	36.33	3.85	341.46	10.64
Altun Shan	2	3	156	1.28	4.13	3.17	294.95	1.40
Eastern Tien Shan	2	1	1243	0.16	12.03	2.59	2440.11	0.49
Hengduan Shan	2	0	700	0.29	26.22	0	1335.39	1.96
Gangdise Mountains	1	0	768	0.13	10.52	0	1339.54	0.79
Dzhungarsky Alatau	0	1	407	0	0	10.98	648.61	0
<b>Total</b>	<b>890</b>	<b>336</b>	<b>35709</b>	<b>2.49</b>	<b>16556.42</b>	<b>3474.60</b>	<b>99817.72</b>	<b>16.59</b>

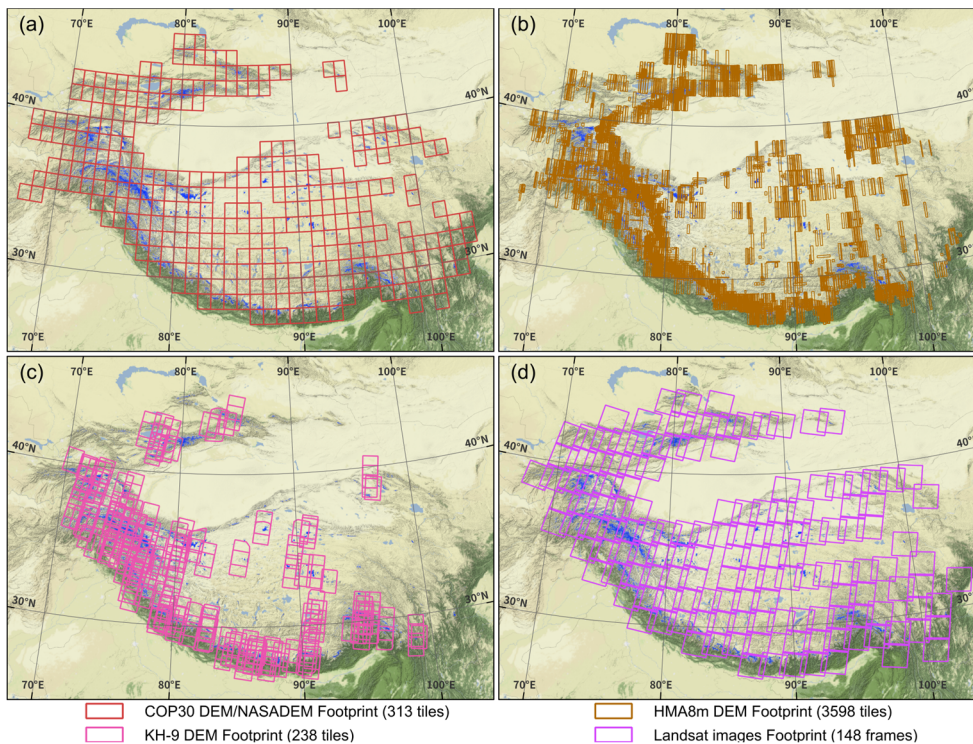
742 \* The value of ratio only considered the number and area of surging glaciers.

743

744 **Table 3: Attribute information in the present surging glacier inventory.**

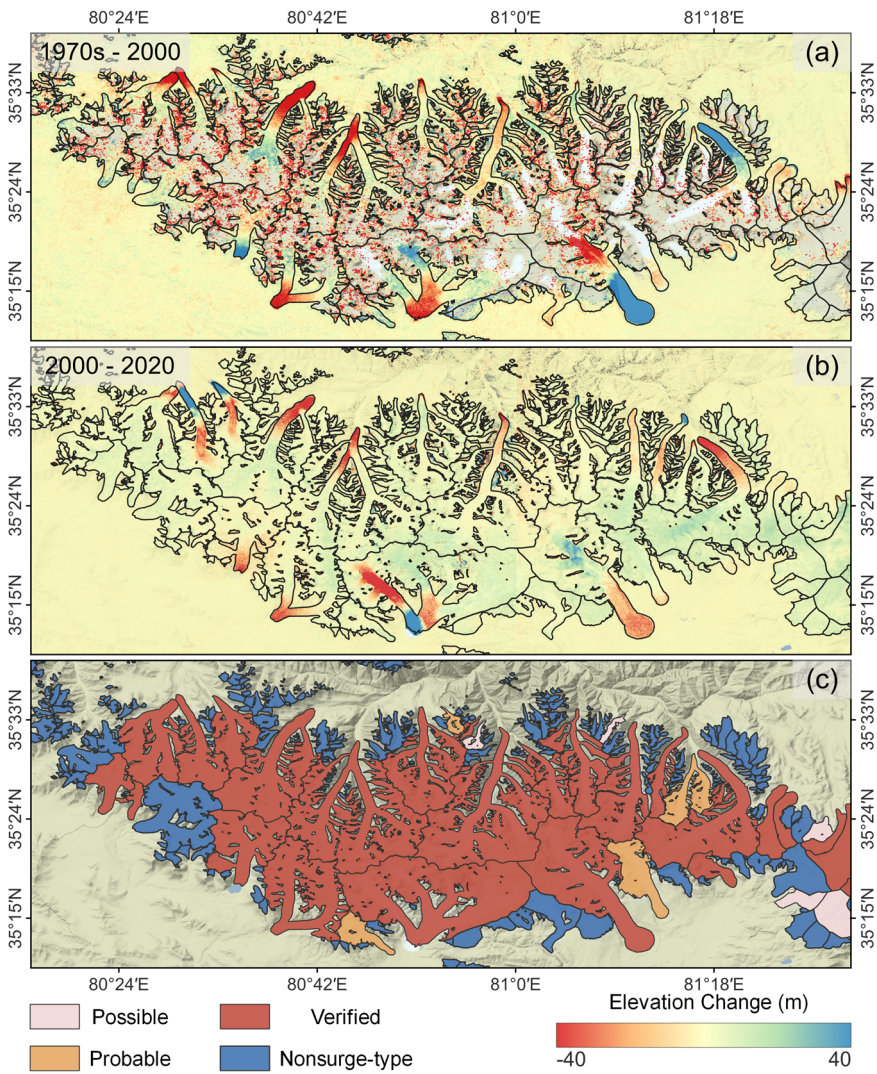
Attribute	Description	Attribute	Description
Glac_ID	Glacier identifier composed by Lat/Lon	Surge_20	Surge identified in 2000-2020 by dH
Area	Glacier area (km <sup>2</sup> )	Surge_70s	Surge identified in 1970s-2000 by dH
Zmin	Minimum elevation of the glacier (m a.s.l)	Delta_T	Identified class of glacier terminus advance
Zmax	Maximum elevation of the glacier (m a.s.l)	Loop_M	Identified class of looped moraine change
Zmed	Median elevation of the glacier (m a.s.l)	Medial_M	Identified class of medial moraine change
Slope	Mean glacier surface slope (°)	False_signal	False positive signal of identification
Aspect	Mean glacier aspect/orientation (°)	Trib_surge	If the glacier has/is surging tributary
MaxL	Maximum length of glacier flow line (m)	Surge_class	Final surge identification during 1970s-2020
HiMAP_region	HMA subregion that the glacier belongs to		

745



746

747 **Figure 1: Footprints of (a) COP30/NASA DEMs, (b) HMA8m DEMs, (c) KH-9 DEMs and (d) Landsat imageries that were utilized**  
748 **in this study. The background is rendered from the ESRI World Physical base map (Source: US National Park Service).**



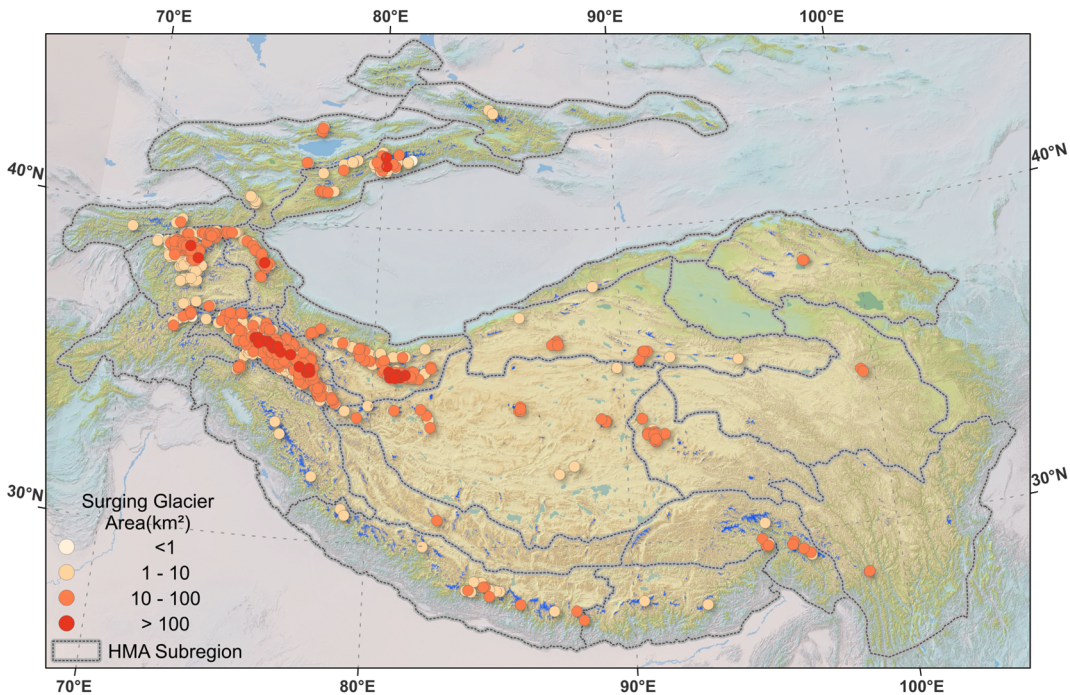
749

750

751

752

**Figure 2: An example of derived elevation change maps during 1970s-2000 (a) and 2000-2020 (b), and the corresponding surging glacier identification result (c). Black curves are glacier outlines. The background is the shaded relief of COP30 DEM (Source: ESA). The area is in the main massif of Western Kunlun Shan.**

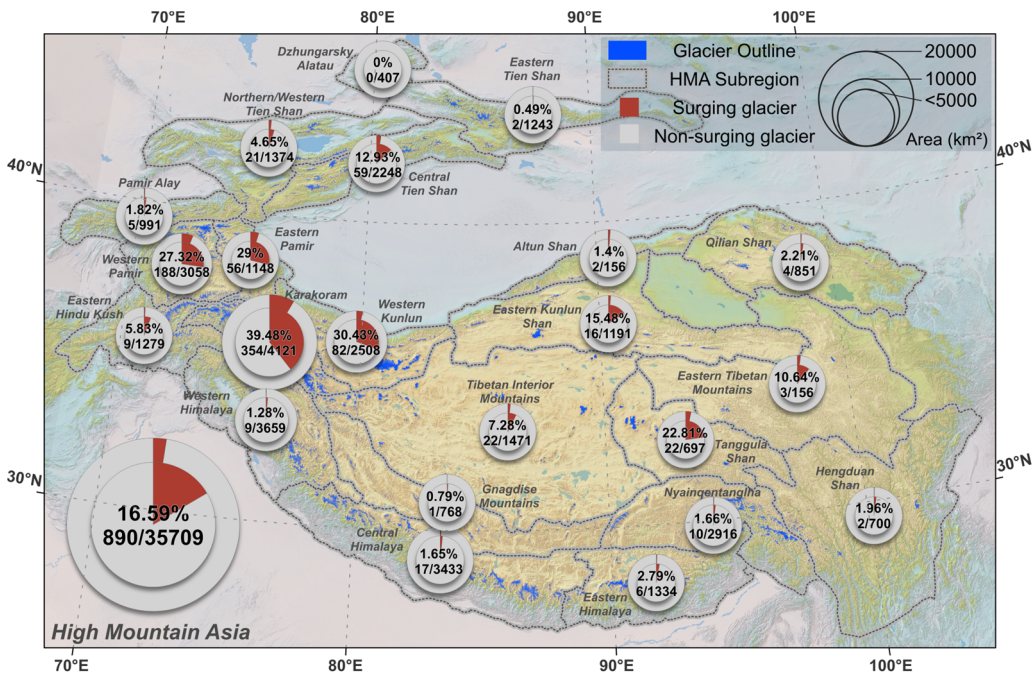


753

754

755

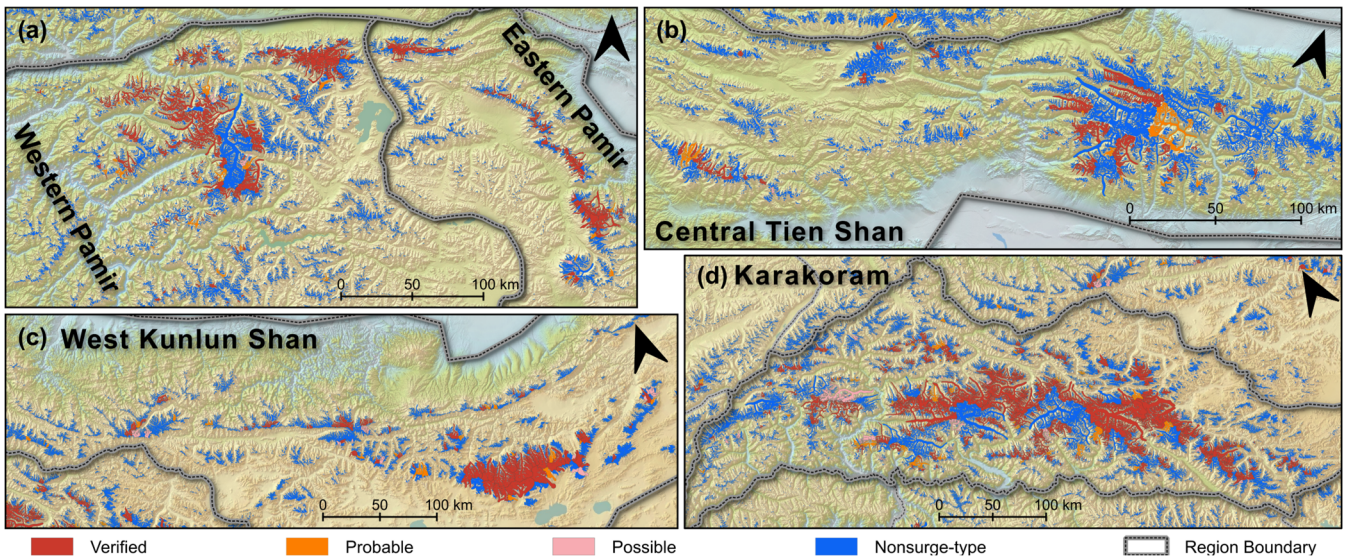
**Figure 3: Overview of the distribution of identified surging glaciers in 22 subregions of HMA. The background is the shaded relief of SRTM DEM (Source: USGS).**



756

757 Figure 4: Distribution of surging glaciers in the 22 subregions of HMA. The double-level pie chart represents the ratios of surging  
 758 glacier number and area in each subregion. The inner pie denotes the area ratio labelled by a percentage, and the outer pie denotes  
 759 the number ratio labelled by a fraction (only considered glacier larger than 0.4 km<sup>2</sup>). The background is the shaded relief of SRTM  
 760 DEM (Source: USGS).

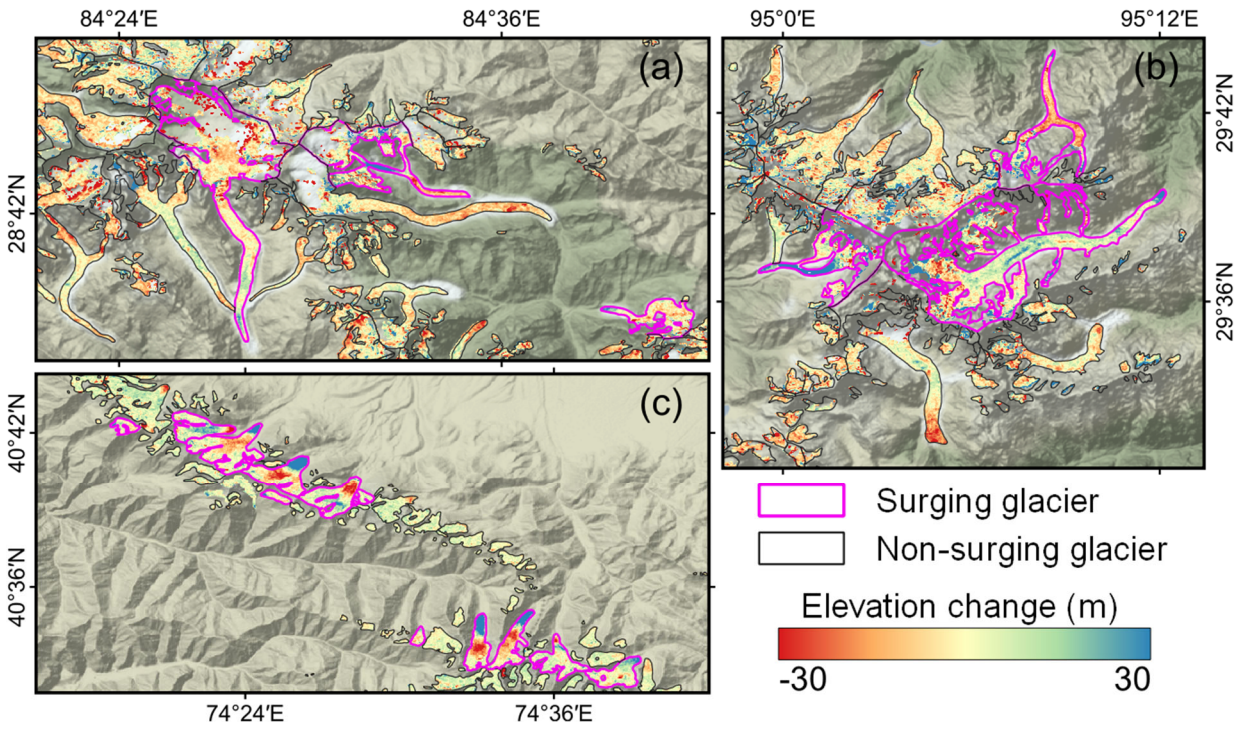
761



762

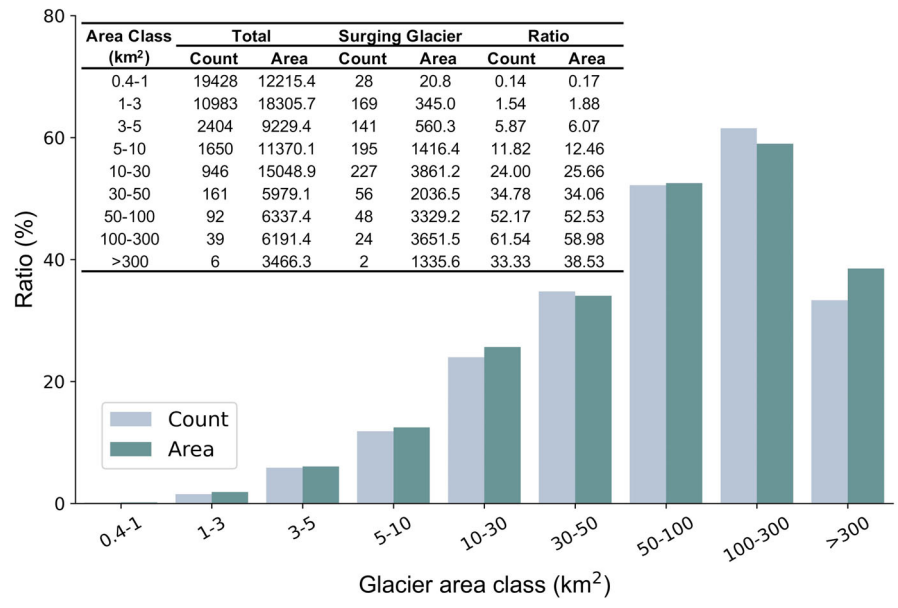
763 Figure 5: Results of surging glacier identification in the Pamirs (a), Central Tien Shan (b), West Kunlun Shan (c), and Karakoram  
 764 (d). The background is the shaded relief of SRTM DEM (Source: USGS).

765

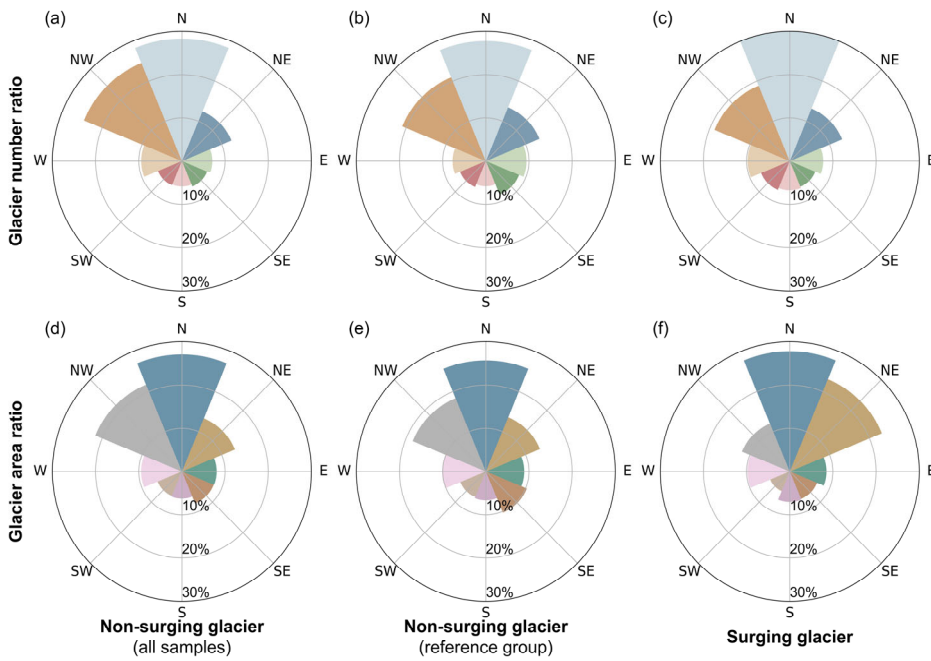


766  
 767 **Figure 6: Elevation change map of identified surging glaciers samples in (a) Central Himalaya (1970s-2000), (b) Nyainqentanglha**  
 768 **(1970s-2000), and (c) Northern Western Tien Shan (2000-2020). Background is the shaded relief of SRTM DEM (Source: USGS).**  
 769 **Note that, surging glaciers presented in the figure were identified by combining multi-temporal elevation change and morphological**  
 770 **changes.**

771



772  
 773 **Figure 7: The ratios of surging glacier number and area in different area classes.**



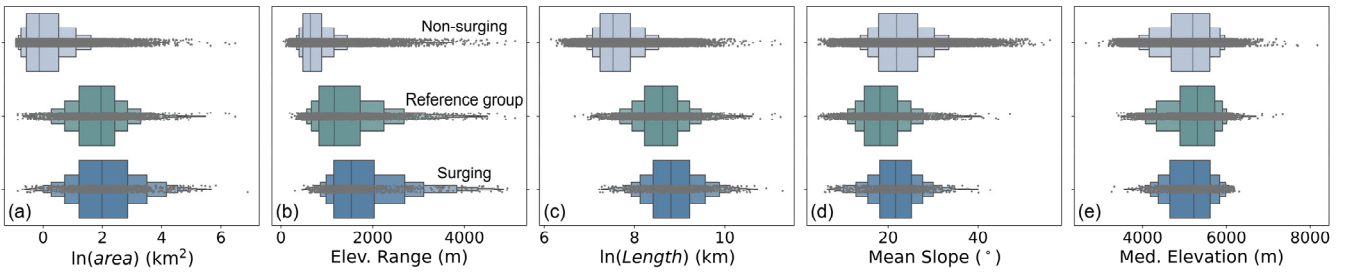
774

775

776

777

**Figure 8: The distribution of glacier number and area in eight aspects. The upper row: glacier number ratio; lower row: glacier area ratio. Left column: distribution of all non-surging glaciers; center column: distribution of non-surging glaciers in the reference group ; right column: distribution of surging glacier. Glaciers smaller than 0.4 km<sup>2</sup> were excluded in the non-surging glacier class.**



778

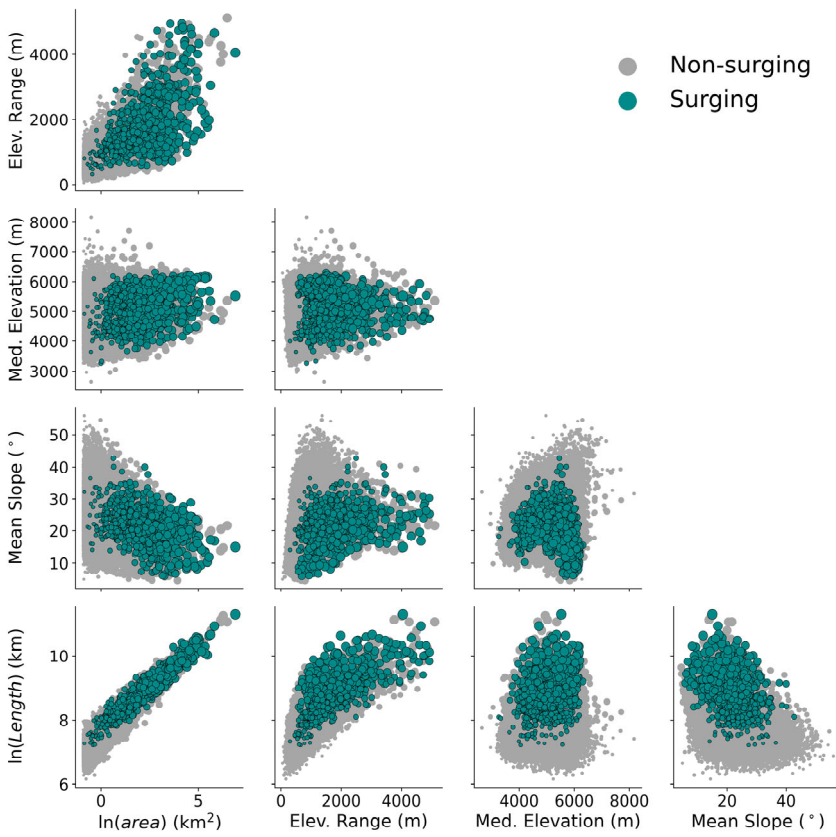
779

780

781

**Figure 9: The comparison between the boxplots of geometric properties of non-surging glaciers (top), non-surging glaciers in reference group (center) and surging glaciers (bottom). (a) Natural logarithm of area. (b) elevation range. (c) Natural logarithm of length. (d) Mean surface slope. (e) Median elevation. Glaciers smaller than 0.4 km<sup>2</sup> were excluded in the non-surging glacier class.**

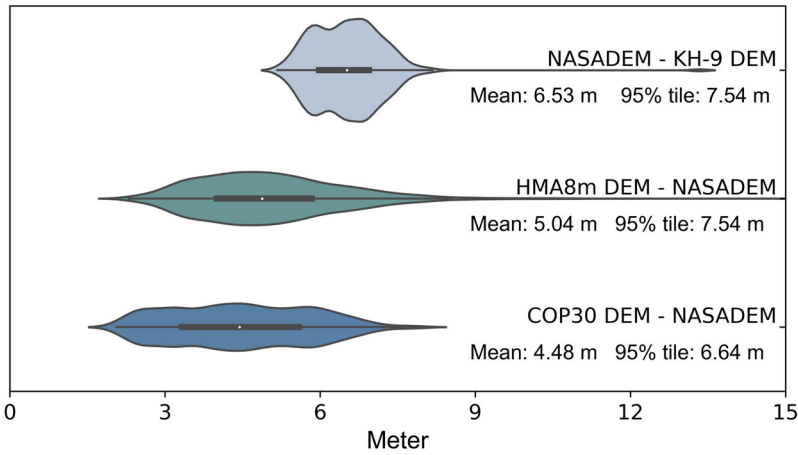




782

783 **Figure 10: Bivariate scatterplots of geometric properties of non-surging and surging glaciers. The larger dots represent larger**  
 784 **glaciers. Glaciers smaller than 0.4 km<sup>2</sup> were excluded in the non-surging glacier class.**

785



786

787 **Figure 11: The distribution of NMAD of elevation change observations in stable areas of all DEM differencing tiles. In each category,**  
 788 **the shaded area denotes the density distribution of the NMAD of all DEM differencing tiles. The white dot denotes the median in**  
 789 **each group. The thick line represents the interquartile range (IQR, i.e., 75th percentile-25th percentile) in each group. The thin line**  
 790 **represents the range between the minimum value (25th percentile - 1.5IQR) and the maximum value (75th percentile + 1.5IQR).**